Phase transformations during cooling from the βZr phase temperature domain in several hydrogen-enriched zirconium alloys studied by in situ and ex situ neutron diffraction

Thai Le Hong, Isabelle Turque, Jean-Christophe Brachet, Jérôme Crépin, Gilles André, Quentin Barres, Raphaëlle Guillou, Caroline Toffolon-Masclet, Jean-Marc Joubert, Matthieu Le Saux

Phase transformations during cooling from the β_{Zr} phase temperature domain in several hydrogen-enriched zirconium alloys studied by *in situ* and *ex situ* neutron diffraction

Thai Le Hong [a, b], Isabelle Turque [a, b, c], Jean-Christophe Brachet [a], Jérôme Crépin [b], Gilles André [d], Quentin Barres [a], Raphaëlle Guillou [a], Caroline Toffolon-Masclet [a], Jean-Marc Joubert [e], Matthieu Le Saux [a, f*]

[a] *DES-Service de Recherches Métallurgiques Appliquées (SRMA), CEA, Université Paris-Saclay, F-91191 Gif-sur-Yvette, France*

[b] *MINES ParisTech, PSL Research University, Centre des Matériaux, CNRS UMR 7633, BP 87, 91003 Evry, France*

[c] *Now at DES-Service d'Etudes des Matériaux Irradiés (SEMI), CEA, Université Paris-Saclay, F-91191 Gif-sur-Yvette, France*

[d] *Laboratoire Léon Brillouin (LLB), CEA, CNRS, Université Paris-Saclay, F-91191 Gif-sur-Yvette, France*

[e] *Université Paris-Est Créteil, CNRS, ICMPE (UMR 7182), 2 rue Henri Dunant, 94320 Thiais, France*

[f] *Now at ENSTA Bretagne, UMR CNRS 6027, IRDL, F-29200 Brest, France*

Abstract

In hypothetical accidental conditions, zirconium-based nuclear fuel claddings can absorb high hydrogen contents (up to several thousand wppm) and be exposed to high temperatures (β_{Zr} phase temperature range) before being cooled. This paper thoroughly investigates the microstructural and microchemical evolutions that take place in such

* Corresponding author.
Email address: matthieu.le_saux@ensta-bretagne.fr (M. Le Saux)

conditions. Two zirconium-based alloys and unalloyed zirconium were pre-charged with hydrogen at various contents up to 3300 wppm and heat-treated at 1000 or 850°C. Neutron diffraction analyses were performed *in situ* upon slow cooling from 700°C and at room temperature. In the materials containing 3300 wppm of hydrogen, β_{Zr} progressively transforms into α_{Zr} during slow cooling then extensively transforms into α_{Zr} and δ_{ZrH2-x} hydrides precipitate via a eutectoid reaction. Thermodynamic predictions at equilibrium are in good agreement with the experimental results. However, depending on the cooling scenario and the average hydrogen content, the precipitation of γ_{ZrH} hydrides, potentially metastable, is evidenced below 350°C and a significant amount of hydrogen can remain in solid solution in α_{Zr}. These metallurgical evolutions and the evolution of the different phase lattice parameters are strongly influenced by the partitioning of oxygen and hydrogen (revealed by electron probe and elastic recoil detection microanalyses) that occurs during the β_{Zr} to α_{Zr} transformation and hydride precipitation.

Keywords: zirconium alloys; hydrogen, β_{Zr} to α_{Zr} phase transformation; eutectoid reaction; *in situ* neutron diffraction

1 Introduction

In pressurized water nuclear reactors, fuel cladding tubes made of zirconium-based alloys are the first barriers that ensure the retention of radioactive fission products. Their mechanical integrity is, therefore, an important issue. Under certain hypothetical accidental conditions such as loss-of-coolant accidents (LOCA), they can be exposed to

steam at high temperature (HT), beyond 700°C typically, up to 1200°C, before being cooled and then quenched in water. Above a temperature depending on the chemical composition of the material and the thermal history, the low-temperature α_{Zr} phase with a hexagonal close-packed (hcp) structure transforms into the HT β_{Zr} phase with a body-centered cubic (bcc) structure [1]. Under specific conditions, the cladding material can absorb a significant amount of hydrogen at HT, up to thousand weight ppm (wppm) locally [2][3][4][5][6][7][9]. Hydrogen mainly concentrates in the β_{Zr} phase [10]. During cooling, the β_{Zr} phase transforms back into the α_{Zr} phase and forms the so-called prior-β_{Zr} structure [11]. The mechanical strength of the cladding during and after cooling mainly results from the mechanical behavior of the residual prior-β_{Zr} layer [12][13]. The mechanical behavior of the (prior-)β_{Zr} structure principally depends on its oxygen and hydrogen contents and on the structural and metallurgical evolutions that take place during cooling from HT [8][10][14]. Several studies addressed the effect of hydrogen on the metallurgical and mechanical behavior of zirconium alloys oxidized at HT. However, most of them focused on hydrogen contents lower than 1000 wppm. For example, it was shown that the higher the hydrogen content below 1000 wppm, the lower the temperature range over which the β_{Zr} to α_{Zr} phase transformation takes place [1][15] and the lower the material ductility at low temperature [10]. Data for materials with higher hydrogen contents and cooled from HT are scarce and often limited to room temperature (RT) [16][17]. Recent results have nonetheless shown that the mechanical behavior of the (prior-)β_{Zr} material is affected by high hydrogen contents up to approximately 3000 wppm in ways that strongly depend on temperature between 20°C and 700°C [13]. In order to interpret such results, it is necessary to have a good knowledge of the microstructural and microchemical evolutions that take place during

cooling from HT. These evolutions for such high hydrogen contents are undoubtedly quite different from those observed for lower hydrogen contents due particularly to a eutectoid reaction expected to occur around 550°C according to the zirconium-hydrogen binary phase diagram [18].

This study aims to improve both experimental database and understanding of the effects of high hydrogen contents, up to 3000 wppm (20 atomic %, at%), on the metallurgical evolutions occurring in zirconium-based alloys during cooling from HT (β_{Zr} phase domain). The effects of the alloy, the average hydrogen content, and the cooling scenario are investigated. X-ray and neutron diffraction analyses were carried out at RT after cooling by applying different scenarios, or *in situ* upon step-cooling from 700°C, on Zircaloy-4 and $M5_{Framatome}$ cladding samples containing 320, 1100-1500 or 3300 wppm of hydrogen. The materials and the experimental procedures used in this study are described in Section 2. The results are presented in Section 3 and then discussed in Section 4. They are compared to thermodynamic predictions at equilibrium obtained using the Thermo-Calc® software together with the Zircobase database [20][21], taking into account all the chemical elements constituting the material (Zr, Nb, Sn, Fe, Cr, H and O). It must be mentioned that, so far, these thermodynamic predictions had not been experimentally validated on multicomponent (multi-alloyed) systems for the highest hydrogen contents studied here.

2 Materials and experimental procedures

2.1 Materials

2.1.1 Zircaloy-4 and M5$_{Framatome}$ cladding tubes

Most specimens were prepared from stress-relieved annealed low tin Zircaloy-4 and fully recrystallized M5$_{Framatome}$ (M5) cladding tube samples, with an outer diameter and a thickness of 9.5 mm and 0.57 mm, respectively. These materials initially contain 0.13-0.14 weight % (wt%) of oxygen and less than 5 wppm of hydrogen. Their nominal chemical compositions are given in wt% in Table 1. In order to investigate the effect of hydrogen, the samples were homogeneously charged with hydrogen at approximately 320, 1100-1500, and 3300 wppm. Hydrogen charging was performed in an argon/hydrogen gas mixture at 400°C to obtain ~300 wppm of hydrogen and, as already done in [13], at 800°C to reach 1100-1500 wppm or 3300 wppm of hydrogen. The samples were then cooled down to RT at a few °C/min.

Table 1

Chemical compositions (in wt%) of the studied materials in as-received conditions (*i.e.* before hydrogen charging).

Material	Sn	Fe	Cr	Nb	O	H	Hf	Zr
Zircaloy-4	1.3	0.2	0.1	< 0.005	0.13	< 0.0005	< 0.006	balance
M5$_{Framatome}$	< 0.005	0.04	< 0.005	1.0	0.14	< 0.0005	< 0.006	balance
Van Arkel Zr	-	0.05	-	-	0.01	0.003	2.2	balance

Hydrogen content measurements were performed using an inert gas fusion thermal conductivity technique (HORIBA EMGA-821 analyzer) on three to seven 2 mm-long ring samples extracted at different locations from the hydrogen-charged cladding

samples, in order to check axial homogeneity of hydrogen. For each sample, measurements were conducted on thirds of the ring samples to verify azimuthal homogeneity of hydrogen. Homogeneity of hydrogen is satisfactory: the variation of hydrogen content along the ~66 mm-long cladding tube samples is typically from a few to a few tens of wppm. Infrared absorption analyses (LECO TC500 analyzer) showed slight oxygen uptake (approximately 0.07 wt%) after hydrogen charging at 800°C, so the samples with 3300 wppm of hydrogen contain approximately 0.2 wt% of oxygen on average.

In order to characterize the properties of the transformed β_{Zr} phase, the samples charged with hydrogen were then heat-treated for a few tens of seconds at about 1000°C in flowing steam. The protective thin oxide layer that grew at the sample surfaces during these heat-treatments allows preventing hydrogen desorption throughout the *in situ* neutron diffraction experiments performed under secondary vacuum at HT and presented below. The total thickness of oxide layer formed during these heat treatments is less than 10 µm. A zone enriched in oxygen with a total thickness of approximately 15 µm was observed beneath the oxide layer. This oxygen-enriched zone represents less than 2% of the whole volume of sample analyzed by neutron diffraction, so it is not expected to have a significant effect on the results. Furthermore, the oxide and oxygen-enriched layers were removed from the samples before being analyzed by X-ray diffraction (XRD), since the analysis depth is limited to a few microns in this case. As shown in Section 3, the results obtained at room temperature by neutron diffraction and XRD were consistent. This confirms that the oxygen-enriched layer has no significant impact on the lattice parameters of the α_{Zr} phase.

With the aim of studying the potential effects of the cooling scenario on the metallurgical evolutions occurring during cooling, several cooling scenarios were applied: direct quenching from 1000°C in water down to RT, slow cooling (0.1-0.4°C/s between 1000 and 500°C, and less than 0.1°C/s below) down to RT or water quenching from 600 or 700°C after cooling at about 0.4-1°C/s from 1000°C. Fig. 1 shows examples of microstructures obtained after cooling. Hydrogen content in the samples was measured after these treatments using HORIBA EMGA-821 analyzer to check the absence of significant desorption or absorption of hydrogen (the oxide layers were not removed before hydrogen analysis).

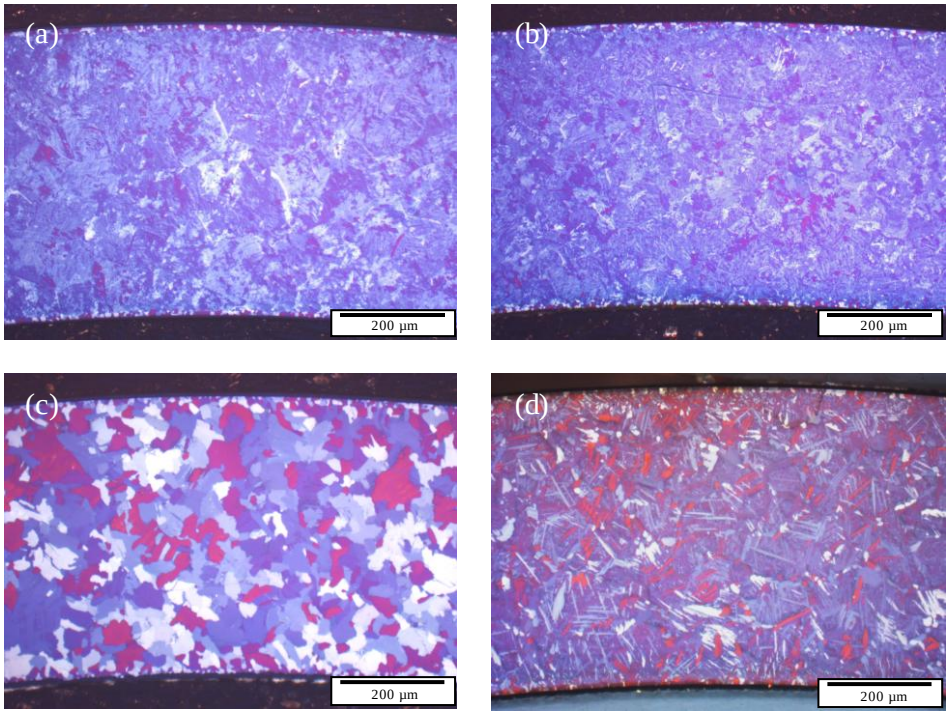

Fig. 1. Polarized optical micrographs of transverse cross-sections of Zircaloy-4 samples heat-treated for a few tens of seconds under steam at 1000°C: (a) hydrogen-free directly water quenched from 1000°C, (b) hydrogen-charged at 320 wppm directly water quenched from 1000°C, (c) hydrogen-charged at 320 wppm cooled at 0.4-1°C/s from 1000°C down to 600°C then water-quenched, (d) hydrogen-charged

at 3300 wppm step-cooled at 0.01°C/s on average from 700°C (after a prior water quenching from 1000°C).

2.1.2 Unalloyed Zr sheet samples

In order to isolate the effects of hydrogen and get rid of the effect of oxygen, several experiments were also performed on 1.2 mm-thick sheet samples of unalloyed zirconium refined using the Van Arkel method (ZrVA), containing only 0.01 wt% of oxygen. 24x14 mm^2 samples without additional hydrogen were heat-treated for a few tens of seconds in flowing steam at 1000°C then directly quenched in water at RT. Hydrogen measurements using the HORIBA EMGA-821 analyzer have shown that the samples absorbed approximately 50 wppm of hydrogen during these treatments.

Other samples with the same dimensions were charged with hydrogen at approximately 3100 wppm under pure hydrogen (99.999 vol%) at 500°C. A strong gradient of hydrogen concentration was observed after this step. A homogenization heat treatment under argon (99.995 vol%) at 800°C was thus applied. It made it possible to limit hydrogen content variations within the samples to only a few tens of wppm for the average hydrogen content of approximately 3100 wppm. Finally, these samples were heat-treated at 850°C (after being encapsulated under argon to avoid oxygen uptake during heat treatment) in order to reach 100% of β_{Zr}, then directly water quenched from 850°C or slowly cooled at an average rate of about 0.3°C/s down to 600°C before being water quenched. According to infrared absorption analyses (LECO TC500 analyzer), the ZrVA samples contain about 0.02-0.04 wt% of oxygen after these treatments.

2.2 Neutron diffraction

Metallurgical evolutions of the materials with temperature during cooling were investigated using neutron diffraction analyses. The neutron diffraction experiments were performed, without further sample preparation, on 50 mm-long Zircaloy-4 and M5 tube samples previously charged with hydrogen and heat-treated at about 1000°C. The analyses were carried out under secondary vacuum at the Léon Brillouin Laboratory (LLB, CEA, CNRS, Université Paris-Saclay, France) on the G4-1 beamline, with a monochromatic thermal neutron radiation and a neutron wavelength of 2.422 Å. A linear multi-detector with 800 cells and a pyrolytic graphite monochromator were used for collection of data in the 2θ range of 12-92° with a step-size of 0.1°, where θ is the Bragg's angle. The neutron beam was perpendicular to the tube axis. The experimental conditions allow neutrons to penetrate the whole volume of the 50 mm-long tube sample.

All the samples mentioned in Section 2.1 were analyzed at RT in order to study the effects of the alloy, the hydrogen content, and the cooling scenario on the final structure and microstructure. The samples containing 3300 wppm of hydrogen were then analyzed *in situ* during step-cooling from 700°C. The sample holder was made of cadmium for *in situ* experiments and in vanadium for experiments performed at RT. The samples were heated at about 1°C/s up to 700°C using a furnace, then held 1h30 at this temperature and finally step-cooled down to RT. The temperature during the experiments was monitored via one thermocouple placed on the sample holder. The temperature gradient in the furnace is expected to be lower than 30°C. An average uncertainty of about ±15°C on the sample temperature is expected for temperatures

above 350°C. Upon cooling, successive isothermal steps were applied, with smaller temperature steps around the expected eutectoid transition: 700, 600, 550, 540, 520, 500, 480, 350, 135, and 40°C. 2h-long steps and data acquisitions were carried out at the different temperatures, except at 700°C and 600°C for which the analyses were limited to 1h30 in order to limit the potential desorption of hydrogen as well as the diffusion of oxygen from the thin zirconia layer to the underlying metal layer at these temperatures. The cooling rate between each step was between 0.25 and 0.03°C/s, leading to a slow average cooling rate of about 0.01°C/s from 700°C to RT. Therefore, the materials could be considered to be close to their thermodynamic equilibrium conditions during the analyses.

It has been observed that the intensity of the continuous background originating from incoherent scattering tends to increase with increasing the average hydrogen content in the sample. No significant evolution of this intensity was observed during the experiments, which suggests that the hydrogen content in the samples did not evolve significantly. The absence of hydrogen desorption was also checked by measuring the hydrogen content after the experiments using the HORIBA EMGA-821 analyzer.

2.3 X-ray diffraction

The influence of hydrogen content on the lattice parameters of α_{Zr} after cooling from the β_{Zr} temperature domain was then investigated using XRD performed at RT on the samples previously analyzed by neutron diffraction. For this purpose, 20 mm-long tube samples were taken from the 50 mm-long Zircaloy-4 and M5 tube samples. In addition, XRD experiments were also conducted at RT on 10x10 mm^2 ZrVA sheet samples

containing low oxygen content, with the aim of isolating the effect of hydrogen. In a second step, XRD analyses were carried out on some of these same samples after annealing them for 24h at 500°C in order to relax the potential residual stresses and dissolve some of the hydrides before cooling from the α_{Zr} domain rather than from the β_{Zr} domain. Before analysis, the samples were mounted and polished by mechanical polishing, followed by chemical etching to remove a thickness of about 100-150 µm at the sample surface, including the ZrO_2 and oxygen-enriched layers formed during heat treatment in steam and the thickness potentially strain-hardened due to polishing.

The XRD experiments were performed in Bragg-Brentano θ-θ geometry on a Bruker D8 Advance diffractometer equipped with a Lynxeye linear detector (3° opening). A monochromatic Cu Kα1 radiation with a wavelength of 1.540598 Å was employed. 6s-long measurements were performed every 0.02° within the 2θ range of 25-140°. Several analyses were also conducted on a PANalytical X'Pert Pro diffractometer using an X'Celerator linear detector (2.122° opening) and a cobalt anticathode with a wavelength of 1.78897 Å. 10s-long measurements were applied with an analysis step of 0.02° within the 2θ range of 10-153°.

2.4 Electron probe microanalysis and micro elastic recoil detection analysis

Electron probe microanalyses (EPMA) were performed using a CAMECA SX100 electron microprobe on selected samples after diffraction analyses to map the main chemical elements including oxygen. Information on the EPMA measurements setup and procedure used in this study can be found in [10]. In addition, micro elastic recoil detection analyses (µ-ERDA) were carried out using a nuclear microprobe at the

Laboratory for Light Element Studies (LEEL, CEA, France) to quantitatively map hydrogen distribution at the microscale [9][22].

3 Results

3.1 Evolutions with temperature during slow cooling

The results obtained by neutron diffraction experiments on metallurgical evolutions occurring during slow cooling are presented below. They are then compared with the thermodynamic predictions at equilibrium obtained using Thermo-Calc and the Zircobase database [20][21]. The comparison will be further discussed in Section 4.

3.1.1 Types of phases

Fig. 2 shows neutron diffraction patterns obtained at different temperatures between 700°C and 500°C or 480°C during step-cooling from 700°C on Zircaloy-4 and M5 containing 3300 wppm of hydrogen heat-treated at 1000°C and water quenched. The two peaks centered at $2\theta = 69°$ and 74° correspond to the cadmium sample holder. Peaks related to monoclinic zirconia m_{ZrO2} ($P2_1/c$ space group) [23] have been observed. As mentioned previously in Section 2.1, the oxide layer was formed during the heat treatment performed in steam at 1000°C before diffraction analysis.

As shown in Fig. 2, between 700°C and 540°C for Zircaloy-4 or between 700°C and 520°C for M5, only peaks corresponding to the two phases, α_{Zr} ($P6_3/mmc$ space group) and β_{Zr} ($Im\bar{3}m$ space group), are observed. During cooling, the intensity of α_{Zr} peaks increases continuously while that of β_{Zr} peaks decreases. This observation highlights the

progressive transformation of β_{Zr} into pro-eutectoid α_{Zr}. The decrease in the intensity of the peak at $2\theta = 55.6°$ does not reveal a decrease in the intensity of the peak corresponding to the (0002) plane of the α_{Zr} phase, which would be an indication of a strong evolution of the texture of the α_{Zr} phase. Actually, this (0002) peak of α_{Zr} is convoluted to the (110) peak of the β_{Zr} phase when the last one exists. Thus, the decrease in the intensity of the peak at 55.6° during cooling above the eutectoid reaction temperatures is considered to be mainly due to a decrease in the intensity of the (110) peak of β_{Zr} as the result of the $\beta_{Zr} \rightarrow \alpha_{Zr}$ phase transformation upon cooling. Indeed, the (110) peak of the β_{Zr} phase is expected to be the most intense one of this phase from 700°C down to the temperature corresponding to the end of the eutectoid reaction. According to the reference diffraction data of zirconium, the (0002) peak of α_{Zr} should not be the most intense one of this phase (which may be the $(10\bar{1}1)$ peak at $2\theta = 58.6°$). Thus, the intensity of the (0002) peak of α_{Zr} is supposed to increase continuously during cooling from 700°C, like the other peaks of this phase, such as $(10\bar{1}0)$, $(10\bar{1}1)$, and $(10\bar{1}2)$. At 500°C for Zircaloy-4, no peak corresponding to the β_{Zr} phase is observed anymore.

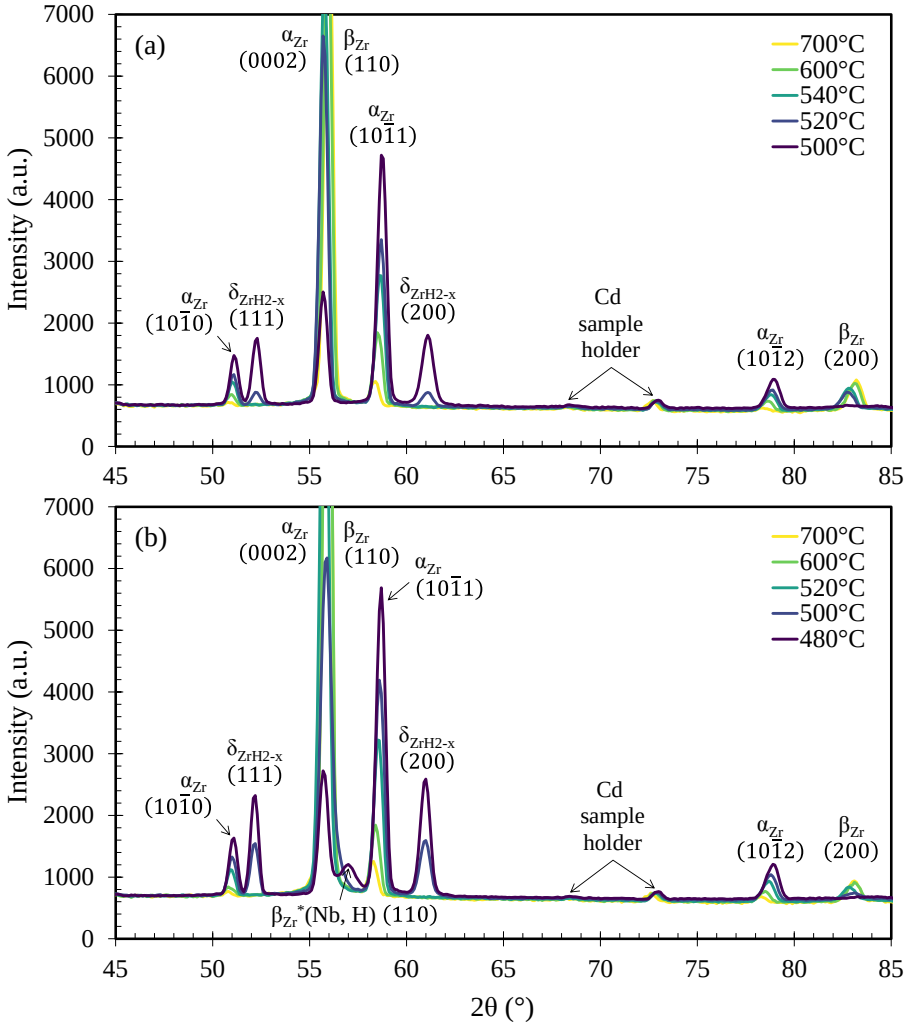

Fig. 2. Neutron diffraction patterns recorded at various temperatures between 700°C and 500°C or 480°C upon step-cooling (0.01°C/s on average) from 700°C for (a) Zircaloy-4 and (b) M5 containing about 3300wppm of hydrogen (and 0.2 wt% of oxygen) water quenched from 1000°C.

Upon the slow step-cooling applied, no peak relative to zirconium hydrides is detected down to 540°C for Zircaloy-4 and 520°C for M5. When the temperature is decreased to about 520°C in the case of Zircaloy-4 and 500°C for M5, peaks of the face-centered cubic δ_{ZrH2-x} hydrides ($Fm\bar{3}m$ space group) appear. The intensity of δ_{ZrH2-x} peaks as well as that of α_{Zr} then rapidly increases upon cooling. At 520°C for Zircaloy-4 and 500°C for M5, the peak corresponding to the (200) plane of β_{Zr} is still present. Thus, the

results show that the three phases α_{Zr}, β_{Zr} and δ_{ZrH2-x} coexist within a temperature range of a few tens of degree:]540°C; 500°C[for Zircaloy-4 and]520°C; 480°C[for M5. Beyond the ±15°C uncertainty on the temperatures considered, an effect of the potential temperature gradient on the width of the temperature range over which the eutectoid transformation takes place cannot be excluded.

The evolution of the phases below 500°C for Zircaloy-4 and 480°C for M5 is illustrated in Fig. 3. In the case of M5, the diffraction diagram highlights the presence of a peak corresponding to the β_{Zr} phase enriched in Nb between the two peaks of α_{Zr} (0002) and $(10\bar{1}1)$. As will be discussed in Section 4, hydrogen may also contribute to the stabilization of this phase at low temperature. This metastable β_{Zr} phase existing below the eutectoid reaction temperatures is denoted β_{Zr}^{*}(Nb, H) in the following so that it can be differentiated from the equilibrium β_{Zr} phase (also enriched in both Nb and H) that only exists above the eutectoid reaction.

It can be seen that during cooling, at temperatures below 500°C for Zircaloy-4 and 480°C for M5, the intensity of δ_{ZrH2-x} peaks continues to increase slightly, due to the decrease of the solubility limit of hydrogen in the α_{Zr} phase and thus the additional precipitation of hydrides. Below 350°C, face-centered tetragonal (fct) γ_{ZrH} hydrides ($P4_2/n$ space group) are detected in both materials. No peak corresponding to the body-centered tetragonal ε hydrides [26] or the hexagonal close-packed ζ hydrides [27] is observed.

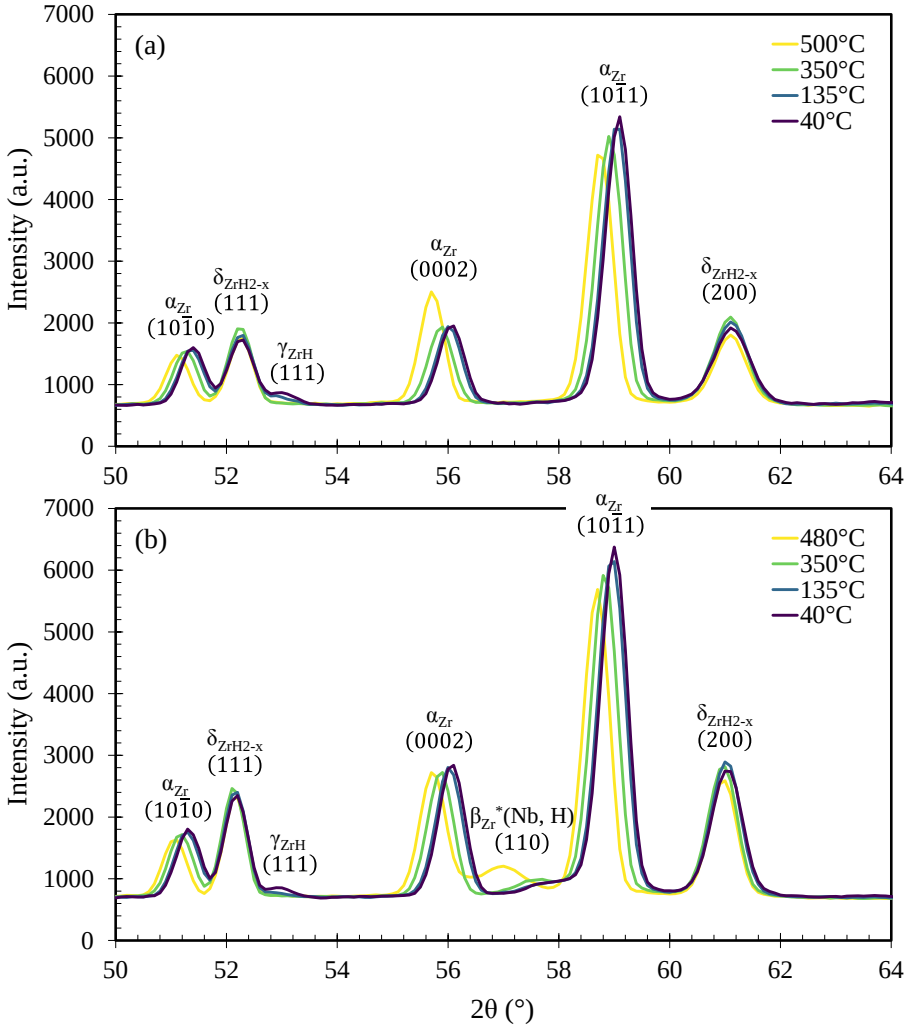

Fig. 3. Neutron diffraction patterns recorded at various temperatures between 500°C or 480°C and 40°C upon step-cooling (0.01°C/s on average) from 700°C for (a) Zircaloy-4 and (b) M5 containing about 3300 wppm of hydrogen (and 0.2 wt% of oxygen) water quenched from 1000°C.

Contrary to expectations [19][20][21][28], the presence of Laves (intermetallic) phases $Zr(Fe, Cr)_2$ (C14-hcp or C15-bcc) in Zircaloy-4 and $Zr(Nb, Fe)_2$ in M5 is not clearly highlighted on diffraction patterns. This may be due to the fact that their fractions are low (< 1 mole %, mol%) and that the most intense peaks of these phases are close to those of the sample holder and those of δ_{ZrH2-x} and γ_{ZrH} hydrides. The bcc β_{Nb} phase expected at low temperature at equilibrium, according to Thermo-Calc + Zircobase

calculations, is not observed on the diffraction diagrams obtained for M5. However, its predicted quantity (0.6 mol%) in equilibrium conditions is likely below the detection limit.

3.1.2 Fractions of phases

The fraction of the phases previously described has been quantitatively determined using the Rietveld refinement method [29] and the Fullprof software. The peaks corresponding to the sample holder have been excluded from the analysis. The refinements did not show the need to explicitly take into account the:

- potential internal stresses (which could be induced by the volume changes associated with the nucleation and growth of the different phases, and by the differences in thermal expansions of these phases),
- microchemical heterogeneities due to solute-element partitioning during the β_{Zr} to α_{Zr} phase transformation,
- slight evolution with temperature of the stoichiometry of δ_{ZrH2-x} hydrides,
- potential effect of hydride morphology (needles, platelets, …),
- hydrogen potentially trapped into the β_{Zr}^{*}(Nb, H) phase stabilized at low temperature in M5,

The α_{Zr} (prior-β_{Zr}) phase resulting from the $\beta_{Zr} \rightarrow \alpha_{Zr}$ transformation upon cooling shows a smooth “fiber” crystallographic texture [30]. This is confirmed by the value of the March-Dollase preferred orientation parameter [31] obtained from the Rietveld analysis, which is slightly higher than 1.

In order to evaluate the potential effects of the texture of the α_{Zr} phase on the phase fractions, Rietveld refinements have been performed by considering different preferred orientations for the α_{Zr} phase: (100), (002), (101), and a combination of the three orientations. The results were not significantly different from those obtained considering an isotropic texture of the α_{Zr} phase: the relative difference in the phase fractions is lower than 5%. Thus, in the following, considering the other sources of uncertainty, it was not necessary to explicitly take into account the texture of this phase.

The stoichiometry of δ_{ZrH2-x} hydrides was fixed at $x = 0.43$, corresponding to the value at RT determined by thermodynamic calculations. γ_{ZrH} hydrides were considered to be stoichiometric. The atomic fraction of Nb in the β_{Zr}^{*}(Nb, H) phase was fixed at 20 at% (equivalent to about 21 wt%). This fraction corresponds to the maximum amount of Nb in β_{Zr} in equilibrium conditions at the monotectoid transition temperature derived from the Zr-Nb phase diagram.

The results in Fig. 4 indicate a good agreement between the calculated and the experimental patterns. This shows that the simplifications made for the quantitative analyses are fully justified.

Fig. 5 shows the fractions of the different phases determined as a function of temperature, for Zircaloy-4 and M5 containing about 3300 wppm of hydrogen. At 700°C, zirconium is mainly in its β_{Zr} phase. The quantitative analyses indicate a small amount of monoclinic zirconia, approximately 1 wt%, detected at all temperatures,

which is consistent with the oxide thickness formed during the heat treatment in steam at 1000°C applied to the samples before diffraction analyses.

The results show that the temperature at which the β_{Zr} phase has fully transformed (into $\alpha_{Zr} + \delta_{ZrH2-x}$ for Zircaloy-4 and $\alpha_{Zr} + \delta_{ZrH2-x} + \beta_{Zr}^{*}$(Nb, H) for M5) is lower by a few tens of °C in the case of M5 compared to Zircaloy-4. The fraction of δ_{ZrH2-x} hydrides in the material at RT is about 34±0.4 mol% for Zircaloy-4 and 36±0.4 mol% for M5, which is consistent with the fact that both alloys contain approximately the same amount of hydrogen on average (about 23±0.05 at%). In the case of M5, a small fraction of approximately 1.8±0.2 mol% of β_{Zr}^{*}(Nb, H) is detected for temperatures below 480°C.

For both Zircaloy-4 and M5, the fraction of γ_{ZrH} increases slightly during cooling from 350°C down to 40°C, but it remains low. In the case of M5, it is about 0.8±0.2 mol% at 350°C and 1.7±0.2 mol% at 40°C. In the case of Zircaloy-4, it is approximately 0.5±0.2 mol% at 350°C. It is about 3.1±0.2 mol% at 40°C, a little bit higher in comparison with M5.

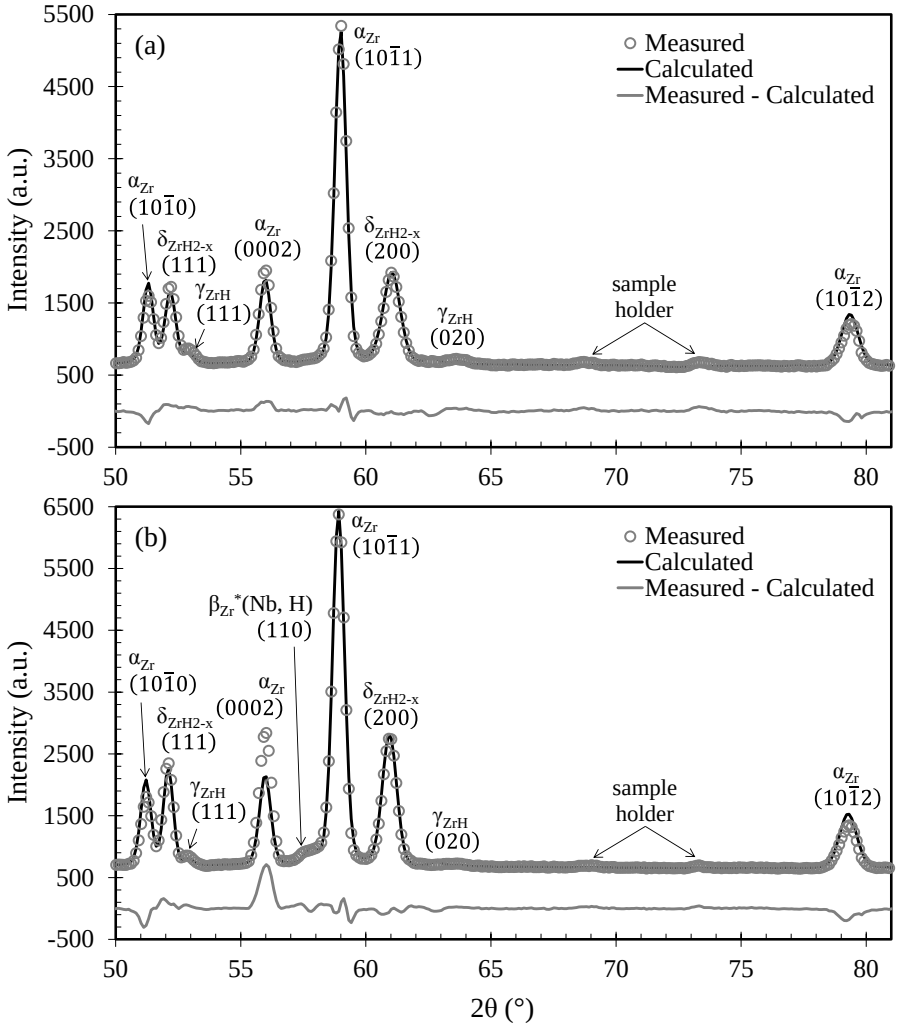

Fig. 4. Rietveld refinement of the neutron diffraction patterns measured at RT after step-cooling (0.01°C/s on average) from 700°C for (a) Zircaloy-4 and (b) M5 containing about 3300 wppm of hydrogen (and 0.2 wt% of oxygen) water quenched from 1000°C.

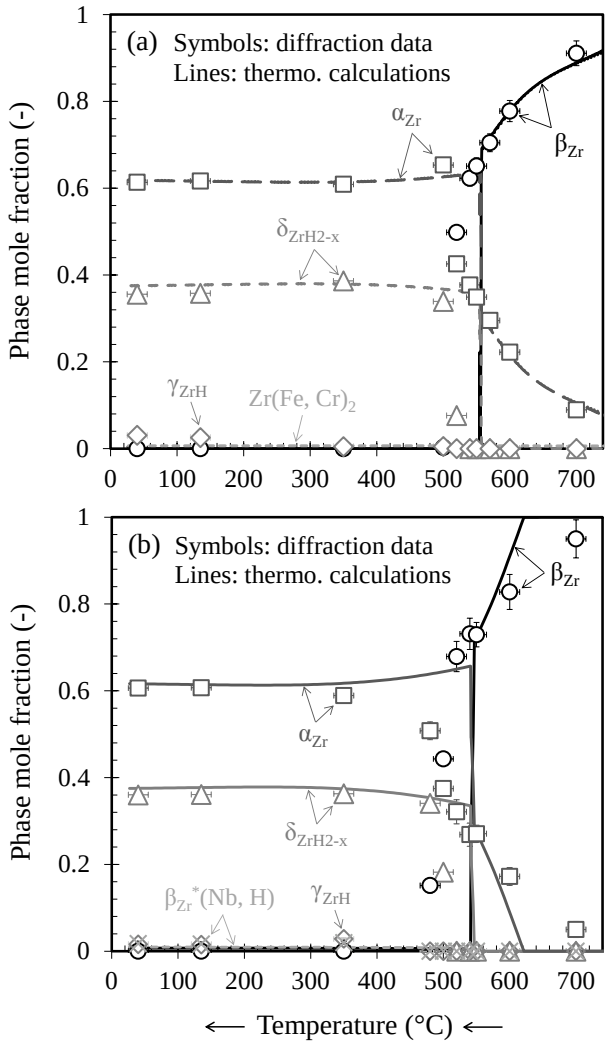

Fig. 5. Evolution of phase mole fractions as a function of temperature obtained by neutron diffraction performed *in situ* during step-cooling (0.01°C/s on average) from 700°C, and by thermodynamic calculations for (a) Zircaloy-4 and (b) M5 containing about 3300 wppm of hydrogen (and 0.2 wt% of oxygen) water quenched from 1000°C.

The amount of hydrogen in solid solution in the material was estimated by calculating the difference between the total hydrogen content measured after the experiments using the HORIBA EMGA-821 analyzer and the quantity of hydrogen in hydrides (δ_{ZrH2-x} and γ_{ZrH}), whose fractions were derived from neutron diffraction data. According to thermodynamic calculations at equilibrium, the hydrogen content in δ_{ZrH2-x} hydrides

increases during cooling. The evolution of the stoichiometry of δ_{ZrH2-x} hydrides predicted by these calculations was taken into account for the estimation of the hydrogen content in solid solution. γ_{ZrH} hydrides were considered to be stoichiometric. Fig. 6 shows that hydrogen is entirely in solid solution at high temperature. In a few tens of °C after hydrides start to precipitate, the fraction of hydrogen in solid solution drops sharply, down to a content lower than 500 wppm. The hydrogen content in solid solution decreases gradually during cooling due to the precipitation of hydrides, down to a few tens of wppm at RT.

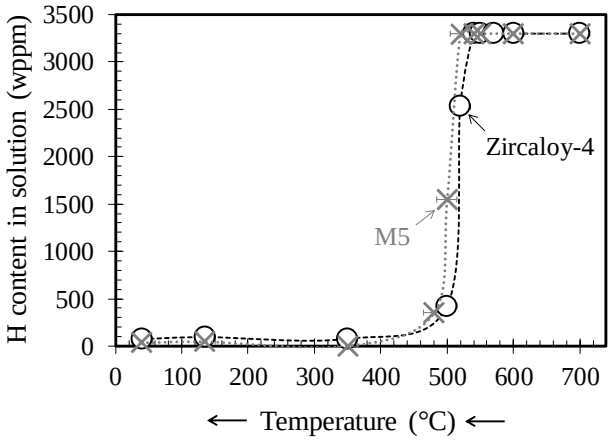

Fig. 6. Evolution of the hydrogen content in solid solution as a function of temperature obtained by neutron diffraction performed *in situ* during step-cooling (0.01°C/s on average) from 700°C on Zircaloy-4 and M5 containing about 3300 wppm of hydrogen (and 0.2 wt% of oxygen) water quenched from 1000°C.

3.1.3 Lattice parameters

Fig. 7 shows the lattice parameters *a* and *c* obtained for the hcp crystal lattice of the α_{Zr} phase. An anisotropic variation of the lattice parameters of this phase as a function of temperature is observed. The parameter *a* of α_{Zr} decreases continuously with decreasing

the temperature upon cooling from 700°C. Below 350°C, the parameter *a* decreases linearly down to RT. At RT, the parameter *a* of M5 is higher than that of Zircaloy-4. The parameter *c* of the α_{Zr} lattice increases when the temperature decreases between 700°C and 540°C or 520°C in the case of Zircaloy-4 or M5, respectively. It decreases progressively at lower temperatures during cooling. Despite this variation of the parameter *c*, the results in Fig. 7 indicate that the volume of the unit cell of this phase decreases progressively during cooling. At 350°C, a change of slope in the evolution of the unit cell volume is noticed. It appears that the α_{Zr} phase contracts in approximately the same way in both materials below 350°C on cooling.

Fig. 8 shows that, for both materials, the lattice parameter of the bcc β_{Zr} phase increases continuously during cooling from 700°C until the end of the eutectoid transformation. This particular evolution is discussed further below.

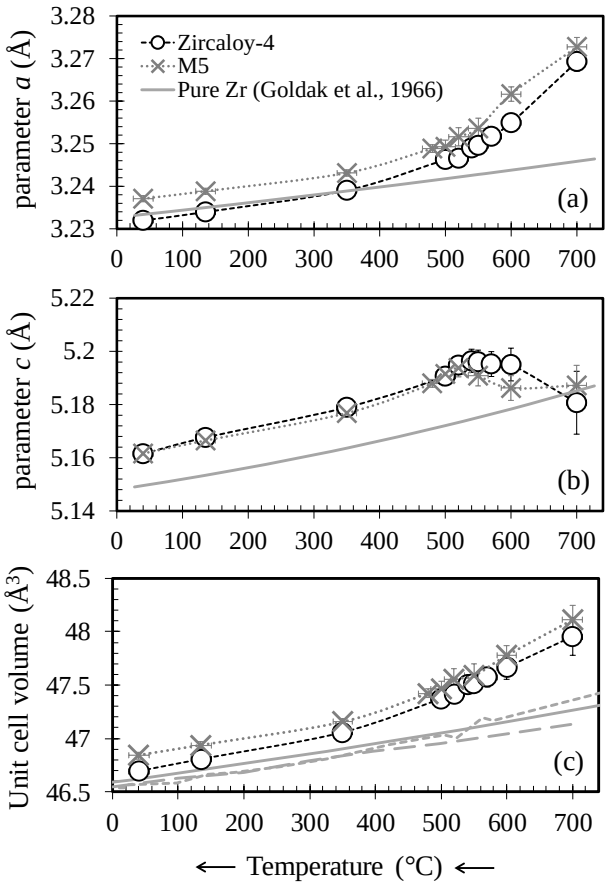

Fig. 7. Evolution of (a) parameter *a*, (b) parameter *c* and (c) volume of elementary cell of the α_{Zr} phase as a function of temperature obtained by neutron diffraction performed *in situ* during step-cooling (0.01°C/s on average) from 700°C on Zircaloy-4 and M5 containing about 3300 wppm of hydrogen (and 0.2 wt% of oxygen) water quenched from 1000°C; comparison to data reported by Russell [32], Couterne and Cizeron [33] and Goldak *et al.* [34] for pure zirconium with almost no hydrogen.

As shown in Fig. 9, in M5, the lattice parameter of the metastable β_{Zr} phase enriched in Nb decreases linearly with the decrease of temperature between 350 and 40°C. The average linear expansion coefficient of this phase between 40 and 350°C determined from these data is equal to $1.08 \cdot 10^{-5}$ K^{-1}.

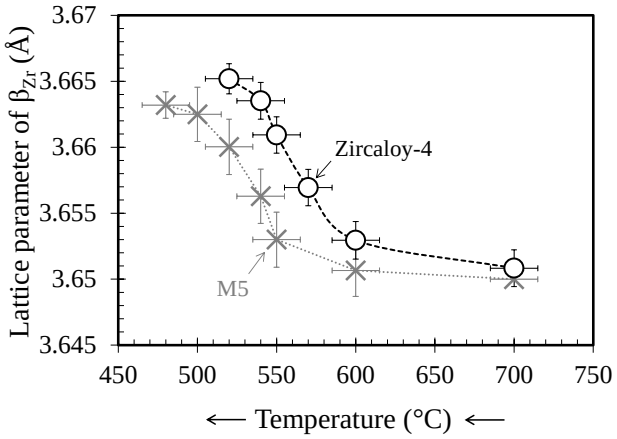

Fig. 8. Evolution of the lattice parameter of the β_{Zr} phase as a function of temperature obtained by neutron diffraction performed *in situ* during step-cooling (0.01°C/s on average) from 700°C on Zircaloy-4 and M5 containing about 3300 wppm of hydrogen (and 0.2 wt% of oxygen) water quenched from 1000°C.

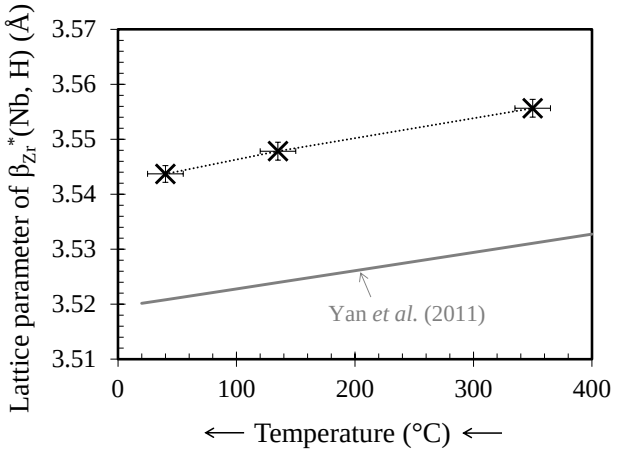

Fig. 9. Evolution of the lattice parameter of the β_{Zr}^{*}(Nb, H) phase as a function of temperature obtained by neutron diffraction performed *in situ* during step-cooling (0.01°C/s on average) from 700°C on M5 containing about 3300 wppm of hydrogen (and 0.2 wt% of oxygen) water quenched from 1000°C; comparison to results from Yan *et al.* [24].

Fig. 10 shows the evolution of the lattice parameter of the fcc δ_{ZrH2-x} hydrides. The lattice parameter decreases slightly with decreasing temperature. This increase is,

nevertheless, significantly smaller than that presented in [35] but in good agreement with those reported in [36] for deuterium-charged zirconium.

The results obtained using neutron diffraction indicate that the lattice parameters of the fct γ_{ZrH} hydrides do not change significantly during cooling below 350°C; they remain constant and equal to a = 4.653±0.001 Å and c = 4.847±0.005 Å.

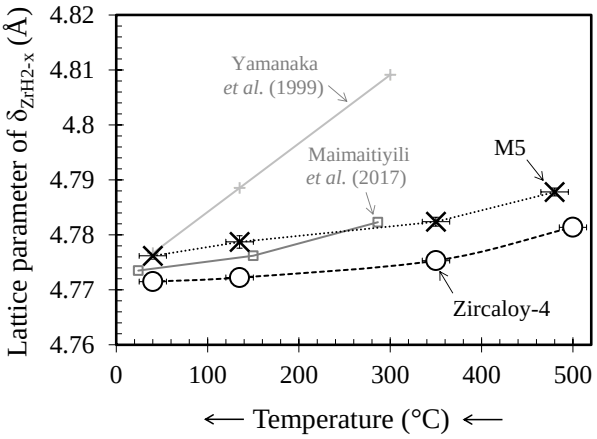

Fig. 10. Evolution of the lattice parameter of δ_{ZrH2-x} hydrides as a function of temperature obtained by neutron diffraction performed *in situ* during step-cooling (0.01°C/s on average) from 700°C on Zircaloy-4 and M5 containing about 3300 wppm of hydrogen (and 0.2 wt% of oxygen) water quenched from 1000°C; comparison to results from Yamanaka *et al.* [35] and Maimaitiyili *et al.*[36].

3.1.4 Distribution of hydrogen and oxygen after cooling

Hydrogen maps obtained by μ-ERDA after the *in situ* neutron diffraction experiments show the presence of zones enriched in hydrogen, with a content up to 6000 wppm on average (about 36 at%), surrounded by hydrogen depleted zones, with a hydrogen content of about 400 wppm on average (4 at%). Comparison with oxygen maps obtained by EPMA shows that the zones depleted in hydrogen are enriched in oxygen,

and *vice versa*. As will be further discussed in Section 4, these microchemical heterogeneities result from the microchemical partitioning between α_{Zr} and β_{Zr} phases that takes place during the β_{Zr} to α_{Zr} phase transformation. The hydrogen-depleted and oxygen-enriched zones are located at the former β_{Zr} grain boundaries. As discussed further in Section 4, these zones likely correspond to the pro-eutectoid α_{Zr} phase formed upon cooling from 700°C before reaching the eutectoid transition temperature.

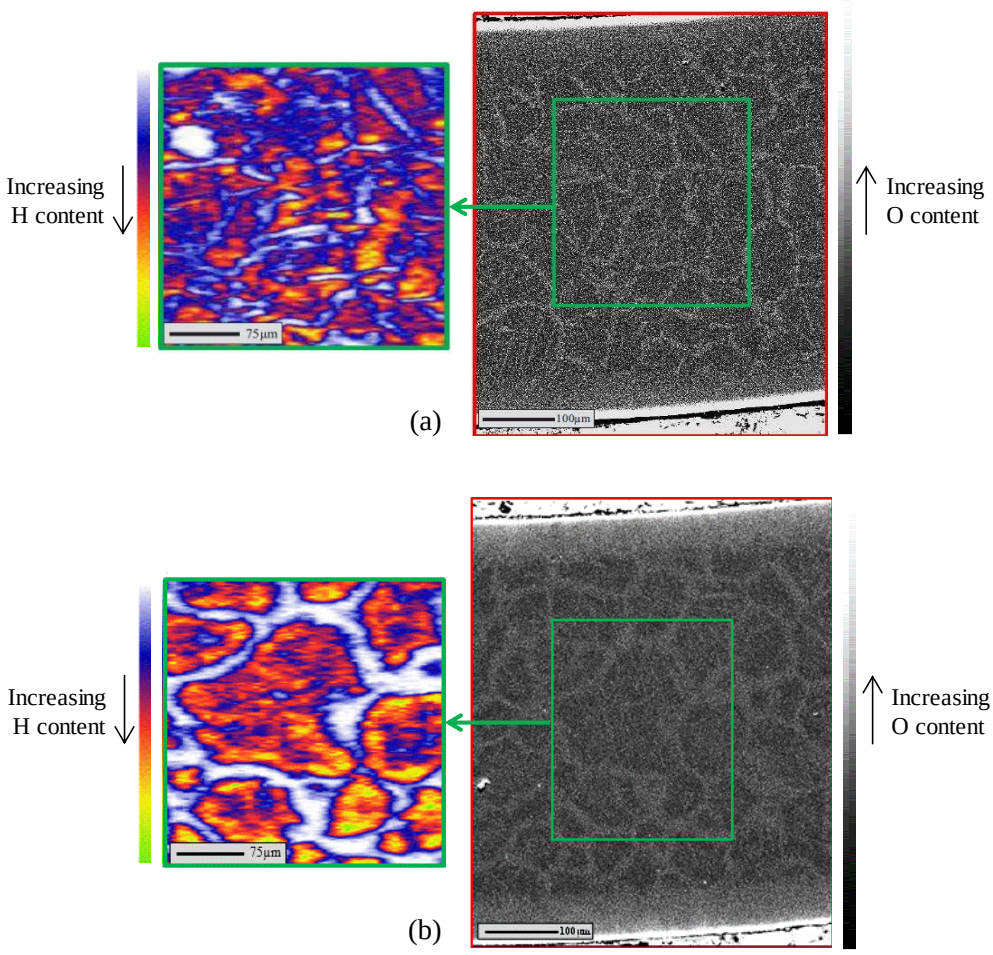

Fig. 11. µ-ERDA map of hydrogen distribution (left) and EPMA map of oxygen distribution (right) at RT of (a) Zircaloy-4 and (b) M5 containing about 3300 wppm of hydrogen (and 0.2 wt% of oxygen) water quenched from 1000°C then step-cooled (0.01°C/s on average) from 700°C.

3.2 Evolutions at RT as a function of hydrogen content and cooling scenario

The results presented above made it possible to quantitatively determine the phase transformations that occur during slow cooling (0.01°C/s on average), *i.e.* under near-equilibrium conditions, from the β_{Zr} phase domain of Zircaloy-4 and M5 containing about 3300 wppm of hydrogen. The effects of the alloy, the hydrogen content, and the cooling scenario on these transformations have also been investigated. For that purpose, in a first step, X-ray and neutron diffraction analyses were performed at RT on:

- Zircaloy-4 and M5 cladding tube samples, as-received or charged with 320, 1100-1500 or 3300 wppm of hydrogen, step-cooled at 0.01°C/s on average from 700°C after water quenching from 1000°C, directly water quenched from 1000°C, or cooled at 0.4-1°C/s from 1000°C down to 600°C then water quenched;
- ZrVA sheet samples, as-received and directly water quenched from 1000°C, or charged with 3100 wppm of hydrogen and heat-treated at 850°C then directly water quenched or quenched from 600°C after cooling at about 0.3°C/s on average.

In a second step, the Zircaloy-4 sample with 3300 wppm of hydrogen step-cooled from 700°C and the ZrVA samples were annealed at 500°C for 24h and then slowly cooled at an average rate of 0.1°C/s down to RT. The samples were then analyzed by XRD at RT. At 500°C, zirconium is entirely in its α_{Zr} phase. The objective was to be closer to the equilibrium hydrides fraction at 500°C.

3.2.1 Types and fractions of phases

Fig. 12 shows neutron diffraction patterns obtained at RT on Zircaloy-4 and M5 containing 320 wppm of hydrogen having undergone direct quenching from 1000°C or quenching from 600°C after cooling at 0.4-1°C/s from 1000°C. On the one hand, no peak related to δ_{ZrH2-x} hydrides is detected after direct quenching. Only peaks corresponding to γ_{ZrH} hydrides are observed, for both materials. On the other hand, after slow cooling from 1000°C down to 600°C then quenching, hydrides are mostly in the δ_{ZrH2-x} phase; only a small amount of γ_{ZrH} is observed.

The fractions of δ_{ZrH2-x}, γ_{ZrH} hydrides, and β_{Zr}^{*}(Nb, H) at RT are shown in Fig. 13 for the different hydrogen contents and cooling scenarios tested for both alloys. The ratio between the fractions of δ_{ZrH2-x} hydrides and γ_{ZrH} hydrides determined after direct water quenching increases with increasing the average hydrogen content. This ratio is higher for M5 than for Zircaloy-4. The faster the cooling, the higher the fraction of γ_{ZrH} hydrides. It reaches about 15 mol% in the material containing 3300 wppm of hydrogen directly quenched from 1000°C. However, in the case of Zircaloy-4 with 3300 wppm of hydrogen, there is no significant difference in the fractions of the hydrides after direct quenching from 1000°C and quenching from 600°C after cooling at 0.4-1°C/s. As shown in Fig. 15, the same observation can be made for ZrVA containing about 3100 wppm of hydrogen: the fractions of the hydrides are in the same order of magnitude after direct quenching from 850°C and after quenching from 600°C after slow cooling from 850°C.

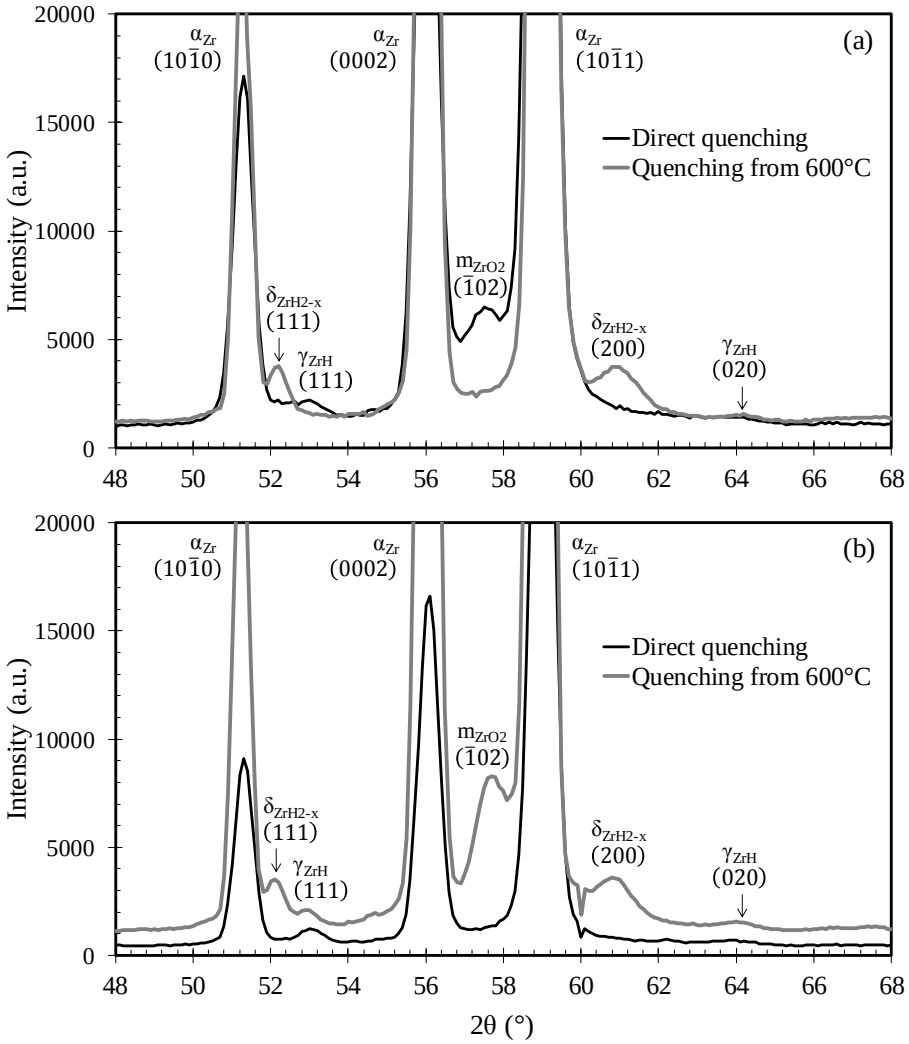

Fig. 12. Neutron diffraction patterns recorded at RT on (a) Zircaloy-4 and (b) M5 containing about 320 wppm of hydrogen after water quenching from 1000°C or cooling at 0.4-1°C/s from 1000°C down to 600°C then water quenching.

Fig. 14 shows the amount of hydrogen remaining in solid solution in the α_{Zr} phase estimated from the total hydrogen content in the material measured using an analyzer and the quantity of hydrogen in hydrides derived from their fraction determined by neutron diffraction. It can be seen that a significant fraction of hydrogen remains in solid solution after direct water quenching from 1000°C. In the case of the materials containing 320 or 1100-1500 wppm of hydrogen, the precipitation of hydrides is

promoted by cooling at 0.4-1°C/s down to 600°C before quenching, compared to direct quenching. In the case of Zircaloy-4 containing 3300 wppm of hydrogen, the hydrogen content remaining in solid solution is not significantly modified by cooling at 0.4-1°C/s down to 600°C before quenching (no diffraction analysis was performed on M5 with the same hydrogen content heat-treated in this condition). However, after step-cooling from 700°C after quenching from 1000°C, almost all hydrogen is precipitated as hydrides (mostly in the form of the δ_{ZrH2-x} phase) at RT; only a small fraction of hydrogen, a few tens of wppm, remains in solid solution after this cooling scenario, which is likely much closer to equilibrium conditions. Fig. 14 indicates that the amount of hydrogen in solid solution at RT after cooling increases with the average hydrogen content for the materials having undergone the same cooling scenario (direct water quenching from 1000°C or water quenching from 600°C). It can reach 850-890 wppm for an average hydrogen content of 3300 wppm. The results suggest that the ratio between the hydrogen content in solid solution and the average hydrogen content decreases with the increase of the average hydrogen content.

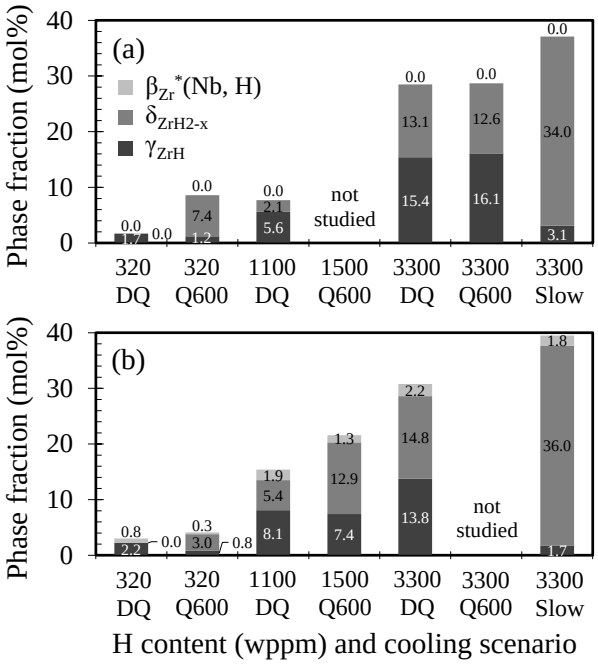

Fig. 13. Phase mole fractions of γ_{ZrH} hydrides, δ_{ZrH2-x} hydrides, and β_{Zr}^{*}(Nb, H) (the fraction of α_{Zr} is not represented; it is such that the total of the fractions of the phases is 100%) in the material at RT determined by neutron diffraction for (a) Zircaloy-4 and (b) M5 containing various hydrogen contents and having undergone various cooling scenarios from 1000°C: direct water quenching from 1000°C (DQ), water quenching from 600°C after cooling at 0.4-1°C/s from 1000°C (Q600), step-cooling at 0.01°C/s on average from 700°C after water quenching from 1000°C (slow).

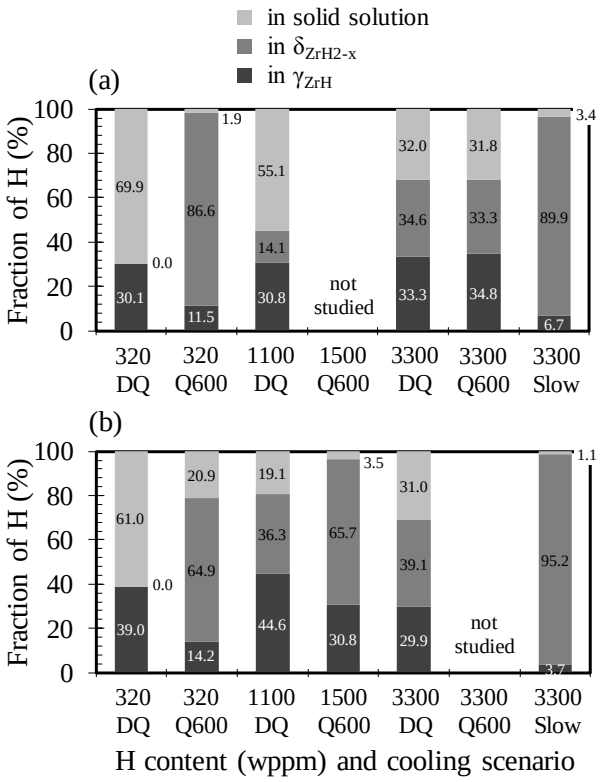

Fig. 14. Percentages of hydrogen in γ_{ZrH} hydrides, δ_{ZrH2-x} hydrides, and in solid solution (in α_{Zr} and/or β_{Zr}^{*}(Nb, H)) in the material at RT determined by neutron diffraction for (a) Zircaloy-4 and (b) M5 containing various hydrogen contents and having undergone various cooling scenarios from 1000°C: direct water quenching from 1000°C (DQ), water quenching from 600°C after cooling at 0.4-1°C/s from 1000°C (Q600), step-cooling at 0.01°C/s on average from 700°C after water quenching from 1000°C (slow).

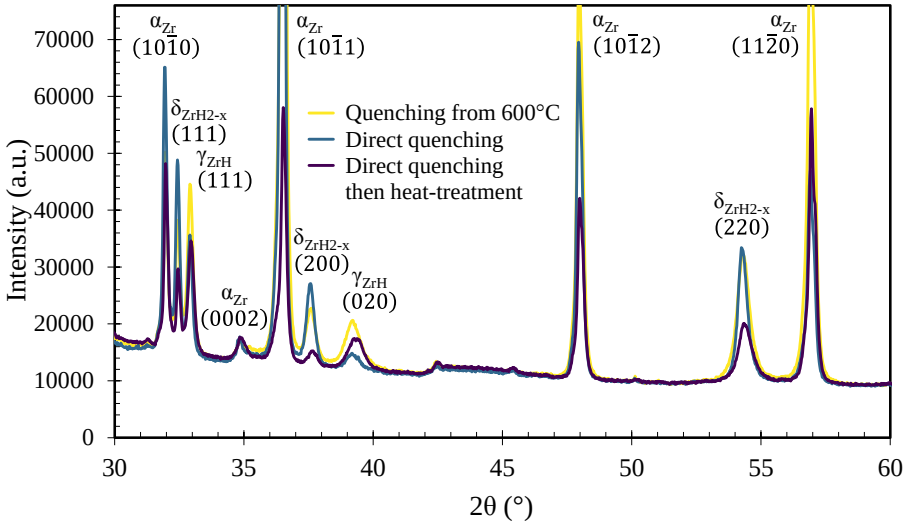

Fig. 15. XRD patterns recorded at RT on ZrVA containing about 3100 wppm of hydrogen subjected to various cooling scenarios: direct water quenching from 850°C, direct water quenching from 850°C followed by a heat treatment for 24h at 500°C, or quenching from 600°C after cooling at about 0.3°C/s on average from 850°C.

The Zircaloy-4 sample with 3300 wppm of hydrogen step-cooled from 700°C and the ZrVA samples with 3100 wppm of hydrogen directly quenched from 850°C or quenched from 600°C were annealed at 500°C for 24h then slowly cooled down to RT. On the one hand, this heat treatment does not significantly modify hydrides' fractions in the case of Zircaloy-4, probably because of a very small hydrogen amount remaining in solid solution after the slow cooling from 700°C. On the other hand, in the case of ZrVA, the heat treatment at 500°C leads to a significant increase in the fraction of γ_{ZrH} hydrides, while the fraction of δ_{ZrH2-x} is not modified. In this case, a significant amount of hydrogen may have remained in solid solution in the α_{Zr} phase after quenching. This hydrogen is thus likely to precipitate in the form of γ_{ZrH} hydrides during the slow cooling from 500°C (*i.e.* upon the second thermal treatment applied).

Fig. 13 shows the evolution of the mole fraction of the β_{Zr}^{*}(Nb, H) phase at RT, determined from neutron diffraction analyses performed on M5 pre-charged at different hydrogen contents from 320 to 3300 wppm and having undergone different cooling scenarios. It can be seen that the higher the hydrogen content and the faster the cooling, the larger the quantity of β_{Zr}^{*}(Nb, H). Furthermore, it seems that the fraction of the β_{Zr}^{*}(Nb, H) phase retained at RT is higher by about 0.4-0.6 mol% after direct quenching from 1000°C than after slow cooling (down to 600°C before quenching or step-cooling from 700°C), regardless of the average hydrogen content.

3.2.2 Lattice parameters

Fig. 16 shows the evolution of the lattice parameters *a* and *c* of α_{Zr} deduced from XRD and/or neutron diffraction analyses carried out at RT as a function of the average hydrogen content for Zircaloy-4, M5, and ZrVA subjected to various cooling scenarios. The lattice parameters' values derived from neutron diffraction and XRD data are consistent. The results in Fig. 16 show that, on the one hand, the parameter *a* does not significantly depend on the cooling scenario and tends to increase slightly with the average hydrogen content for the three materials tested. On the other hand, the parameter *c* increases considerably with the average hydrogen content, in particular for Zircaloy-4 and M5. The value of the parameter *c* is slightly higher after direct quenching from 1000°C (in the case of Zircaloy-4) or 850°C (in the case of ZrVA) than after quenching from 600°C after slow cooling or step-cooling from 700°C. The evolution of the lattice parameters with the average hydrogen content is smaller after slow cooling down to 600°C followed by water quenching than after direct quenching.

In the case of Zircaloy-4 containing 3300 wppm of hydrogen step-cooled from 700°C, the lattice parameters of α_{Zr} at RT are not significantly changed after a heat treatment for 24h at 500°C followed by a slow cooling at about 0.1°C/s down to RT. However, in the case of ZrVA containing 3100 wppm of hydrogen directly quenched from 850°C, the lattice parameters of α_{Zr} are significantly decreased after this heat treatment, and they approach those measured on the hydrogen-free sample.

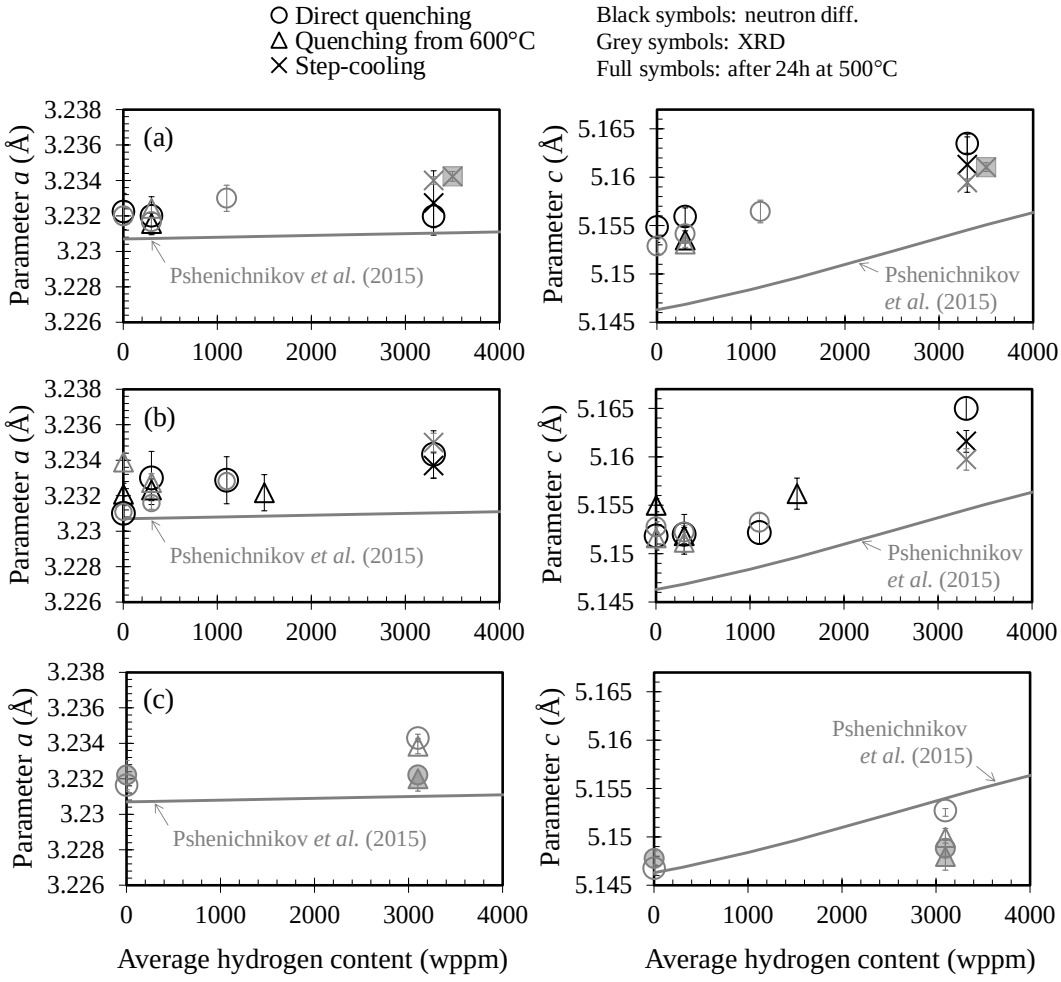

Fig. 16. Evolution of the lattice parameters of the α_{Zr} phase as a function of the average hydrogen content obtained at RT by neutron diffraction and XRD on (a) Zircaloy-4, (b) M5, and (c) ZrVA subjected to various cooling scenarios: direct water quenching from 1000 or 850°C, direct water quenching from 1000 or 850°C followed by a heat treatment for 24h at 500°C, water quenching from 600°C after cooling at

0.4-1 or 0.3°C/s from 1000 or 850°C, or step-cooling at 0.01°C/s on average from 700°C after water quenching from 1000°C; comparison to data reported by Pshenichnikov *et al.* [16] for Zircaloy-4.

4 Discussion

4.1 Comparison of experimental results and thermodynamic predictions

Fig. 5 compares the fractions of phases determined by neutron diffraction upon step-cooling (0.01°C/s on average) from 700°C and those predicted by the thermodynamic calculations at equilibrium, for Zircaloy-4 and M5 containing 3300 wppm of hydrogen (and 0.2 wt% of oxygen). It is shown that the experimental data are in good agreement with the thermodynamic predictions, for the equilibrium phases in particular, *i.e.* α_{Zr}, β_{Zr}, and δ_{ZrH2-x} (Fig. 5). The largest difference between thermodynamic predictions and experimental data is observed for M5 at 700°C. It is important to recall that these calculations had not been experimentally validated for such high hydrogen contents so far. The γ_{ZrH} hydride phase, potentially metastable, was not taken into account in the thermodynamic calculations at equilibrium. The temperatures at which the eutectoid reaction occurs, according to the neutron diffraction data, are lower by about 20-30°C compared to those predicted by equilibrium calculations. Furthermore, the temperature ranges over which this reaction takes place, according to neutron diffraction, are wider by about 35°C. This makes sense because of a hysteresis effect during cooling relative to the equilibrium temperatures. This difference would probably be more significant for faster cooling due to dynamic effects.

4.2 Microchemical evolutions during cooling

As presented in Section 3.1.4, the materials show microchemical heterogeneities after cooling. As developed hereafter, the zones less rich in hydrogen and richer in oxygen must correspond to those firstly transformed into pro-eutectoid α_{Zr} during cooling, preferentially at the former β_{Zr} grain boundaries. The zones very rich in hydrogen and less rich in oxygen should correspond to the residual zones of β_{Zr} that were not transformed when reaching the eutectoid reaction temperature.

These micro-chemical heterogeneities result from the partitioning of the chemical elements during the phase transformation of zirconium during cooling. Above the eutectoid transition temperature, hydrogen is distributed between α_{Zr} zones and β_{Zr} zones. These zones evolve during the on-cooling pro-eutectoid β_{Zr} to α_{Zr} phase transformation. Fig. 17 shows the evolutions, with temperature, of the hydrogen and the oxygen contents in solid solution in the α_{Zr} and β_{Zr} phases predicted by thermodynamic calculations at equilibrium for Zircaloy-4 containing 3300 wppm of hydrogen. The tendencies are similar for M5. The oxygen content in solid solution is higher in the α_{Zr} phase than in the β_{Zr} phase as a result of the α_{Zr}-stabilizing effect of oxygen. During cooling from 700°C down to the eutectoid transition temperature, the oxygen content in solid solution decreases in both the pro-eutectoid α_{Zr} phase and the β_{Zr} phase, due to the β_{Zr} to α_{Zr} phase transformation (increase of the fraction of the α_{Zr} phase) and the α_{Zr}-stabilizing effect of oxygen (enrichment and depletion of oxygen in the α_{Zr} phase and the β_{Zr} phase respectively). During cooling above the eutectoid transition temperature, the hydrogen content in solid solution increases in both the α_{Zr} phase and the β_{Zr} phase. However, the hydrogen content is much higher in the β_{Zr} phase where it can reach approximately 5300 wppm as against about 400 wppm in the pro-eutectoid α_{Zr} phase.

These contents are in good agreement with those determined by μ-ERDA (Fig. 11) in the presumed prior-β_{Zr} zones transformed during the eutectoid reaction and pro-eutectoid α_{Zr} zones.

In the following discussion, the potential effects of internal stresses are not considered, as these stresses have not been measured. Beyond their direct effect on the lattice parameters, these stresses may play an indirect role via a potential effect on the chemical partitioning during the on-cooling phase transformation. However, if it exists, this effect of stresses on chemical partitioning does not seem to be significant, since the chemical compositions measured after cooling by EPMA and μ-ERDA are close to the thermodynamic predictions at equilibrium without taking into account stress effects.

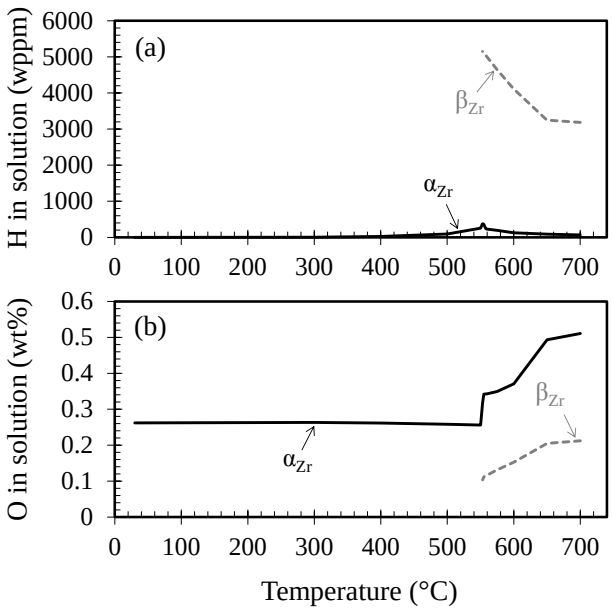

Fig. 17. Evolution with temperature of (a) the hydrogen content and (b) the oxygen content in solid solution in the α_{Zr} phase and the β_{Zr} phase determined from thermodynamic calculations at equilibrium, for Zircaloy-4 containing about 3000 wppm of hydrogen (and 0.2 wt% of oxygen).

4.3 β_{Zr} phase

The evolution of the lattice parameter of the β_{Zr} phase has been determined between 700°C and 520 or 480°C for Zircaloy-4 and M5 containing 3300 wppm of hydrogen. The vast majority of the data reported in the literature on the evolution of the lattice parameter or the thermal expansion of this phase as a function of temperature are limited to temperatures superior to 900°C [37][38], *i.e.* above the range investigated in this study. However, lattice parameter values of 3.604 Å at 627°C [39] and 3.627 Å at 700°C [40] have been reported for pure hydrogen-free β_{Zr}. These values are approximately 0.02 to 0.05 Å lower than those determined in this study for Zircaloy-4 and M5 containing 3300 wppm of hydrogen. This difference is probably due to the additional chemical elements, notably hydrogen, present in the materials studied.

The results in Fig. 8 show that the lattice parameter of the β_{Zr} phase increases with decreasing the temperature between 700°C and 520 or 480°C. The contraction of purely thermal origin is thus outweighed by other effects. On the one hand, according to the thermodynamic calculations shown in Fig. 17, the oxygen content in solid solution in the β_{Zr} phase decreases during cooling down to the eutectoid reaction temperature. Thus, the evolution of the lattice parameter of β_{Zr} cannot be explained by the evolution of its oxygen content. On the other hand, the hydrogen content in solid solution in the β_{Zr} phase increases continuously during cooling in this temperature range. Hence, the evolution of the lattice parameter of the β_{Zr} phase as a function of temperature above the eutectoid reaction temperatures can be a direct result of the effect of a progressive enrichment in hydrogen of this phase upon cooling.

4.4 β_{Zr}^{*}(Nb, H) phase in M5

In the case of M5, a residual (metastable) β_{Zr} phase noted β_{Zr}^{*}(Nb, H) has been highlighted at low temperatures. The fraction of this phase at RT is higher after direct quenching than after slow cooling. The existence of a β_{Zr} phase enriched in Nb retained at RT in the form of stringers between α_{Zr} laths was reported in [19] for Zr-2.5%Nb heat-treated for 5 min at 1045°C then slowly cooled at an average rate of 0.05°C/s. This can be explained by the fact that below 700°C, Nb diffuses very slowly, which favors the stabilization of a significant fraction of a metastable β_{Zr} phase containing theoretically up to ~20 wt% of Nb [19][24]. It can be assumed that hydrogen has an additional effect. It should prevent the decomposition of the β_{Zr} phase enriched in Nb by delaying the on-cooling β_{Zr} to α_{Zr} phase transformation as the result of its β_{Zr}-stabilizing effect. Indeed, this decomposition involves the diffusion (partitioning) of niobium, whose rate decreases with decreasing the temperature. Moreover, hydrogen, which concentrates in the last β_{Zr} zones to be transformed on cooling, could have an intrinsic chemical effect by stabilizing a higher proportion of the metastable β_{Zr} phase retained until RT. Thus, this β_{Zr}^{*}(Nb, H) phase is expected to be enriched in both Nb and H, hence the notation used.

The Nb content is not expected to evolve in this phase between 350 and 40°C because of its very slow thermal diffusion. Therefore, it can be supposed that the evolution of the lattice parameter of this phase (Fig. 9) with temperature is mostly of thermal origin. The value of the linear expansion coefficient of this phase estimated between 40 and 350°C, previously mentioned in Section 3.1.3, is in good agreement with the thermal expansion coefficient of the β_{Zr} phase, which is generally determined at much higher

temperatures. The values of the lattice parameter of the β^*_{Zr}(Nb, H) phase obtained in this study are higher by about 0.024 Å than those reported in [24] for Zr-2.5%Nb analyzed by neutron diffraction during heating at 0.3°C/s between RT and 500°C and then at 0.03°C/s between 500 and 1000°C. This difference is consistent with the one observed on the lattice parameter of the β_{Zr} phase at 700°C between M5 hydrogen-charged at 3300 wppm and pure hydrogen-free zirconium, as previously mentioned in Section 4.3.

4.5 Hydrides and hydrogen in solid solution

The results have shown that, for hydrogen contents higher than about 1000 wppm, δ_{ZrH2-x} hydrides precipitate upon (slow) cooling from the β_{Zr} temperature domain, mainly during the eutectoid reaction. The observed evolution, with temperature, of the lattice parameter of this phase is assumed to result from, at least, two phenomena: thermal expansion and possible evolution of their stoichiometry. In addition, the precipitation of γ_{ZrH} hydrides has been evidenced below approximately 350°C. No evolution of the lattice parameters of γ_{ZrH} with temperature has been observed, knowing that no such evolution has been reported so far in the literature. ε hydrides [26] or ζ hydrides [27] have not been observed in this study.

The coexistence of γ_{ZrH} and δ_{ZrH2-x} hydrides upon cooling has already been reported in the literature [16][25][41][42][43][44][45][46][47]. Several authors suggested that γ_{ZrH} hydrides are stable at temperatures below 250-280°C [42][45][46]. The disappearance of a large or even a total fraction of γ_{ZrH} hydrides has been noted in [45][46] at temperatures above 180°C on heating. The reverse phenomenon was observed during cooling from 400°C, but the fraction of precipitated γ_{ZrH} hydrides is much lower than

that estimated before heating. This was recently confirmed through *in situ* neutron diffraction experiments performed on the Zr-D system [47][48]. Root *et al.* [45] suggested that the formation of γ_{ZrH} hydrides is associated with the partial dissolution of δ_{ZrH2-x} hydrides. This transformation would be energetically favorable due to the smaller elementary cell volume of γ_{ZrH} compared to that of δ_{ZrH2-x}, thus minimizing micro-stress. Bailey [49] observed only γ_{ZrH} hydrides in zirconium containing between 100 and 1000 wppm of hydrogen directly quenched in ice-cold salt-water or rapidly cooled down from 800°C. Pshenichnikov *et al.* [17] suggested that, for hydrogen contents close to 100 wppm and below, the formation of γ_{ZrH} hydrides is favored due to the low hydrogen content, which would not allow the precipitation of δ_{ZrH2-x} hydrides. For the high hydrogen contents investigated here in this study, the formation of γ_{ZrH} hydrides could be related to the partition of oxygen and hydrogen during the β_{Zr} to α_{Zr} transformation. As shown in Section 3.1.4, there are zones with very high hydrogen content surrounded by areas containing less hydrogen. Therefore, γ_{ZrH} hydrides could preferentially form near the areas with the lowest hydrogen content.

It has been shown that a certain fraction of hydrogen remains in solid solution in the α_{Zr} phase after cooling from the β_{Zr} temperature domain down to RT. These observations are in agreement with those of Pshenichnikov *et al.* [16] who reported that a part of the hydrogen, up to 400 wppm, would remain in solid solution after cooling in air from 727°C at a rate of about 5°C/s, for Zircaloy-4 containing 2250 to 4760 wppm of hydrogen on average. Trapping of hydrogen in solid solution at low temperature is not predicted by thermodynamic calculations at equilibrium.

4.6 α_{Zr} phase

As shown in Fig. 7, the evolutions of the lattice parameters of the α_{Zr} phase between 700°C and ~500°C in Zircaloy-4 and M5 containing 3300 wppm of hydrogen are very different from those observed in the materials with little hydrogen. Above the eutectoid reaction temperature, the value of the parameter *a* is higher and its decrease with decreasing temperature is more significant than those reported in [32], [33], and [34] for pure α_{Zr} containing almost no hydrogen (< 10 wppm). In this temperature range, the parameter *c* increases with decreasing temperature in the case of Zircaloy-4 and M5 containing 3300 wppm of hydrogen, while it decreases in the case of pure hydrogen-free zirconium. Below 350°C, the evolutions of the parameters *a* and *c* as a function of temperature are similar to those reported in [32], [33], and [34]. These results suggest that, as for the β_{Zr} phase, the variations of the lattice parameters of α_{Zr} with temperature are not purely of thermal origin in the materials investigated in this study. As shown in Section 3.1.4, there is a microchemical partition between the pro-eutectoid α_{Zr} phase and the β_{Zr} phase during the on-cooling β_{Zr} to α_{Zr} transformation. Note that no significant partitioning of tin is expected in Zircaloy-4 for the conditions studied here [50].

Fig. 17 shows that the hydrogen content in solid solution in the α_{Zr} phase increases during cooling above the eutectoid reaction temperatures, while its oxygen content decreases. Oxygen is known to induce an anisotropic expansion of the lattice parameters of α_{Zr} [51][52]. However, based on the results of Boisot and Béranger [51], it can be concluded that the evolution of the oxygen content determined here cannot be insufficient to explain the evolution of the lattice parameters observed. Thus, in the

temperature range of 700-540°C, the decrease of the parameter *a* of the pro-eutectoid α_{Zr} phase is dominated by thermal effects [33][53] that outweigh the effects of the evolutions in hydrogen and oxygen contents in solid solution. Hydrogen atoms are bigger than the volume of the tetrahedral sites of the α_{Zr} phase in which they are inserted [54][55], leading to an expansion of the α_{Zr} lattice [56]. Therefore, the increase of the parameter *c* observed during cooling between 700 and 540°C (Fig. 7) probably results from the insertion of hydrogen atoms that outweighs the contraction of purely thermal origin. In summary, the present results show a very anisotropic effect of the insertion of hydrogen atoms within the hcp lattice of the pro-eutectoid α_{Zr} phase above the eutectoid reaction temperatures.

It has been observed that the lattice parameters of the α_{Zr} phase at RT, in particular the parameter *c*, increase with increasing the average hydrogen content (Fig. 16). It is important to remind that Zircaloy-4 and M5 samples charged with hydrogen at 3300 wppm contain about 0.2-0.3 wt% of oxygen on average due to a slight oxygen uptake during hydrogen charging at 800°C (as mentioned in Section 2.1.1), while the oxygen content in hydrogen-free materials is 0.13-0.14 wt%. However, according to the results of Boisot and Béranger [51], the difference in average oxygen contents cannot simply explain the increase of 0.006-0.009 Å in the parameter *c* measured between the hydrogen-free samples and the samples containing 3300 wppm of hydrogen. The lattice parameters' values of the α_{Zr} phase measured for hydrogen-free ZrVA in this study are similar to those given for pure zirconium in the Powder Diffraction File™ provided by the International Centre for Diffraction Data (a = 3.232 Å and c = 5.147 Å). The lattice parameters determined for hydrogen-free Zircaloy-4 and M5 at RT are in good

agreement with those reported by Stern *et al.* [52] for Zircaloy-4 containing 0.25 wt% of oxygen. However, they are higher than those reported in [16] for Zircaloy-4, which are, curiously, very close to the lattice parameters measured for hydrogen-free ZrVA (unalloyed). Although the lattice parameters' values are shifted, the relative increase of the lattice parameters of α_{Zr} with increasing the average hydrogen content is consistent with the observation made by Pshenichnikov *et al.* [16]. This increase seems to be related to the residual hydrogen content in solid solution at RT, which is higher after direct quenching than after slower cooling, as shown in Fig. 13.

The results presented in Section 3.2.2 show that, in the case of ZrVA, the lattice parameters of the α_{Zr} phase at RT do not evolve any more with the average hydrogen content after a heat treatment at 500°C promoting the precipitation of hydrides (Fig.16). In this case, the (anisotropic) expansion of the α_{Zr} lattice observed at RT in the presence of hydrogen would, therefore, be entirely due to the residual hydrogen in solid solution. However, in the case of Zircaloy-4 and M5, the lattice parameters of α_{Zr} increase with increasing the average hydrogen content even after very slow cooling, for which only a very small quantity of hydrogen remains in solid solution at RT (< 100 wppm). It is difficult to imagine that this increase in the lattice parameters of α_{Zr} is due to a direct effect of hydrogen almost entirely precipitated in the form of hydrides. It can be assumed that, in alloyed materials as Zircaloy-4 and M5, hydrogen has an indirect effect on the evolution of the lattice parameters of α_{Zr} by inducing the enrichment, notably in oxygen, of certain zones of the matrix (partitioning) during the phase transformations occurring on cooling from the β_{Zr} phase domain. Stern *et al.* [52] observed such an effect of oxygen partitioning in oxygen-enriched materials cooled from the β_{Zr} phase

domain. In particular, they observed a shift and/or a doubling of XRD peaks related to the presence of microchemical (oxygen) heterogeneities.

5 Conclusions

This paper provides a detailed quantitative description of the microstructural and microchemical evolutions that take place during cooling from the β_{Zr} temperature domain in zirconium alloys containing up to very high hydrogen contents. For that purpose, X-ray and neutron diffraction analyses were performed *in situ* upon slow cooling (about 0.01°C/s on average) from 700°C or *post facto* at RT after various cooling scenarios from 1000°C. The experiments were conducted on Zircaloy-4 and M5 cladding samples as well as on unalloyed zirconium sheet samples (in particular, with almost no oxygen), pre-charged with hydrogen at different contents up to 3300 wppm. The distribution of chemical elements, in particular oxygen and hydrogen, in the samples was quantitatively determined after cooling by EPMA and μ-ERDA. The experimental results were systematically compared to thermodynamic predictions at equilibrium obtained using Thermo-Calc associated with the Zircobase database, taking into account all the elements constituting the materials. The main conclusions of this work can be summarized as follows:

1. In the materials containing 3300 wppm of hydrogen, the β_{Zr} phase progressively transforms into the pro-eutectoid α_{Zr} phase during cooling at ~0.01°C/s on average, down to 540°C for Zircaloy-4 or 520°C for M5. The lattice parameter of the β_{Zr} phase increases significantly during cooling from 700°C to about 500°C. This is likely due to the increase of the hydrogen content in solid solution in this phase during the on-cooling β_{Zr} to α_{Zr} phase transformation,

outweighing the opposite thermal (contraction) effect. The parameter *a* of the α_{Zr} lattice decreases with decreasing temperature above the eutectoid transformation temperatures, but the parameter *c* increases and reaches its maximum value at the eutectoid transition temperatures. These anisotropic evolutions of the lattice parameters of the α_{Zr} phase can be explained by the competition between the effect of thermal contraction and that of the increase in the hydrogen content in solid solution in the α_{Zr} phase in this temperature range. The first effect is preponderant on the evolution of the parameter *a*. The second one is preponderant on the evolution of the parameter *c*. Despite this anisotropic evolution of the lattice parameters of α_{Zr}, the elementary cell volume of the crystal lattice decreases during cooling in these temperature ranges, and the effect of thermal contraction outweighs the effect of chemical segregation at the level of the crystal lattice volume.

2. Below 540°C for Zircaloy-4 and 520°C for M5, both containing 3300 wppm of hydrogen, the residual β_{Zr} phase rapidly transforms into α_{Zr}. δ_{ZrH2-x} hydrides extensively precipitate via a eutectoid reaction:
    - $\beta_{Zr} \longrightarrow \alpha_{Zr} + \delta_{ZrH2-x}$ in the case of Zircaloy-4,
    - $\beta_{Zr} \longrightarrow \alpha_{Zr} + \beta_{Zr}^{*}(Nb, H) + \delta_{ZrH2-x}$ in the case of M5.

    The decomposition of β_{Zr} is not complete in the case of M5: residual β_{Zr} enriched in Nb and H, noted $\beta_{Zr}^{*}(Nb, H)$, remains at low temperatures. Therefore, α_{Zr}, β_{Zr}, and δ_{ZrH2-x} phases coexist between 540 and 500°C for Zircaloy-4 and between 520 and 480°C for M5, cooled at 0.01°C/s on average. Thermodynamic calculations at equilibrium also predict the existence of these

domains but in temperature ranges higher by about 20-30°C and narrower by about 35°C, which is likely due to a cooling hysteresis effect.

3. The mole fractions of phases determined from quantitative analyses of the diffraction data obtained upon slow cooling at an average rate of 0.01°C/s are in good agreement with those predicted by thermodynamic calculations at equilibrium. It is important to notice that thermodynamic predictions had not yet been experimentally validated for the high hydrogen contents investigated in this study.
4. Hydrides mainly precipitate during the eutectoid reaction in the form of δ_{ZrH2-x} hydrides. However, they continue to precipitate at lower temperatures due to the decrease of the solubility limit of hydrogen in the α_{Zr} phase with decreasing temperature upon cooling. In addition, γ_{ZrH} hydrides precipitate below 350°C for both Zircaloy-4 and M5. This phase is observed at RT in all the samples containing 320, 1100-1500 and 3300 wppm of hydrogen, after direct water quenching from 1000°C as well as after slower cooling (cooling at 0.4-1°C/s from 1000°C down to 600°C then water quenching, or step-cooling from 700°C at 0.01°C/s on average). After direct quenching, γ_{ZrH} hydrides are in the majority compared to δ_{ZrH2-x} hydrides. The fraction of δ_{ZrH2-x} hydrides at RT increases with decreasing the cooling rate. The higher the average hydrogen content, the larger the ratio between the fractions of δ_{ZrH2-x} hydrides and γ_{ZrH} hydrides after direct water quenching. The precipitation of γ_{ZrH} hydrides could be associated with the partitioning of oxygen and hydrogen during the phase transformation of zirconium during cooling, leading to the presence of zones with a hydrogen

content up to 6000 wppm surrounded by areas containing typically a few hundreds of wppm of hydrogen.

5. A significant amount of hydrogen remains in solid solution in the α_{Zr} phase after cooling down to RT. The higher the average hydrogen content and the faster the cooling rate, the higher the hydrogen content remaining in solid solution. For example, 850-890 wppm (~8 at%) of hydrogen is still dissolved in the α_{Zr} phase after direct quenching from 1000°C in the materials containing 3300 wppm of hydrogen on average.
6. For the M5 alloy, the higher the average hydrogen content or the faster the cooling rate, the more significant the mole fraction of metastable β_{Zr}^{*}(Nb, H) stabilized at RT.
7. After cooling from the β_{Zr} temperature domain, the parameter *c* and, to a lesser extent, the parameter *a* of the α_{Zr} lattice increase with increasing the average hydrogen content in Zircaloy-4 and M5 at RT. The faster the cooling rate, the higher the value of the parameter *c*. The lattice parameters of unalloyed zirconium (ZrVA) evolve in approximately the same way as for Zircaloy-4 and M5. After heat-treatment at 500°C for 24h followed by slow cooling at 0.1°C/s on average, the lattice parameters of the α_{Zr} phase of ZrVA charged with hydrogen become equivalent to those of the hydrogen-free material. In this case, the expansion of the α_{Zr} lattice in the presence of hydrogen is entirely attributed to the hydrogen remaining in solid solution after cooling. In the case of alloyed materials, *i.e.* Zircaloy-4 and M5, it is assumed that in addition to the direct effect of hydrogen, the expansion of the lattice parameters of α_{Zr} is associated

with an indirect effect of hydrogen, via its influence on the distribution of other elements, notably oxygen.

Fig. 18 summarizes the main microstructural and microchemical evolutions, highlighted in this study, that occur during cooling from the β_{Zr} temperature domain in Zircaloy-4 and M5 containing more than 1000 wppm of hydrogen. The case of the materials containing 3300 wppm of hydrogen is considered by way of illustration.

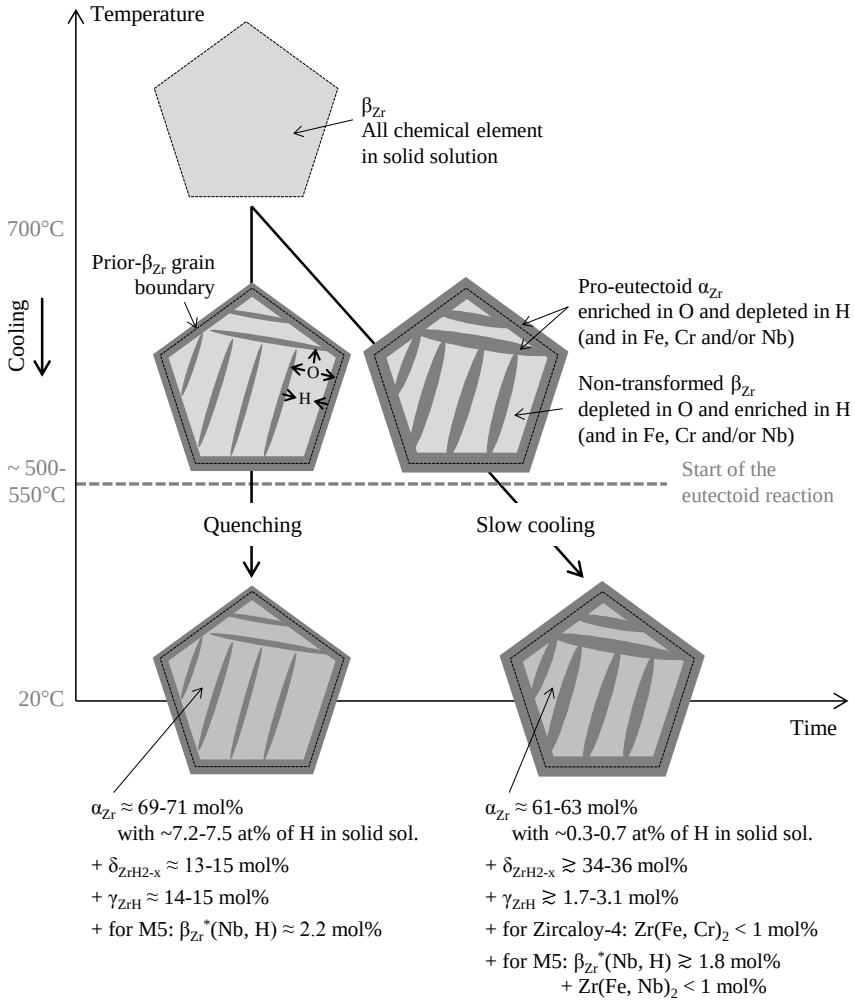

Fig. 18. Schematic representation of the metallurgical and microchemical evolutions occurring during cooling from the β_{Zr} temperature domain down to RT, in Zircaloy-4 and M5 containing 3300 wppm of

hydrogen; comparison of the microstructures obtained at RT after direct water quenching from 1000°C and after slow step-cooling at 0.01°C/s on average (even if not represented, a small fraction of hydrides probably precipitates during cooling in prior-pro-eutectoid α_{Zr} zones, which contain a few tens to a few hundreds of wppm of hydrogen).

6 Acknowledgements

The authors thank F. Damay from LLB (CEA, CNRS), P. Berger and C. Raepsaet from LEEL (CEA), P. Bossis from DEN-DMN (CEA), C. Cobac, T. Guilbert, A. Lequien, G. Nony, J. Roubaud and S. Urvoy from DEN-SRMA (CEA), J.D. Bartout from MINES ParisTech, F. Couturas and M. Dottor from ICMPE (UPEC, CNRS), and EDF and Framatome, for their contributions to this work. This work was funded by the French Nuclear Institute in the framework of the GAINES project.

References

[1] J.C. Brachet, L. Portier, T. Forgeron, J. Hivroz, D. Hamon, T. Guilbert, T. Bredel, P. Yvon, J.P. Mardon, P. Jacques, Influence of hydrogen content on the α/β phase transformation temperatures and on the thermal-mechanical behavior of Zy-4, M4 (ZrSnFeV), and M5™ (ZrNbO) alloys during the first phase of LOCA transient, Zirconium in the Nuclear Industry: 13th International Symposium, ASTM STP 1423, American Society for Testing and Materials, West Conshohocken, PA, 2002, pp. 673-701.

[2] H.M. Chung, T.F. Kassner, Embrittlement Criteria for Zircaloy Fuel Cladding Applicable to Accident Situations in Light-water Reactors. Summary Report, NUREG/CR-1344, ANL-7948, Argonne National Laboratory, Lemont, IL, 1980.

[3] H. Uetsuka, T. Furuta, S. Kawasaki, Failure-bearing capability of oxidized Zircaloy-4 cladding under simulated loss-of-coolant condition. Journal of Nuclear Science and Technology 20 (1983) 941-950.

[4] M. Billone, Y. Yan, T. Burtseva, R. Daum, Cladding Embrittlement during Postulated Loss-of-Coolant Accidents. NUREG/CR-6967, Argonne National Laboratory, Lemont, IL, 2008.

[5] F. Nagase, T. Chuto, H. Uetsuka, Behavior of High Burn-up Fuel Cladding under LOCA Conditions. Journal of Nuclear Science and Technology 46 (2009) 763-769.

[6] J. Stuckert, M. Große, C. Rössger, M. Klimenkov, M. Steinbrück, M. Walter, QUENCH-LOCA program at KIT on secondary hydriding and results of the commissioning bundle test QUENCH-L0. Nuclear Engineering and Design 255 (2013) 185-201.

[7] R. Thieurmel, J. Besson, E. Pouillier, A. Parrot, A. Ambard, A.F. Gourgues-Lorenzon, Contribution to the understanding of brittle fracture conditions of zirconium alloy fuel cladding tubes during LOCA transient. Journal of Nuclear Materials 527 (2019) 151815.

[8] H.M. Chung, A.M. Garde, T.F. Kassner, Development of an Oxygen Embrittlement Criterion for Zircaloy Cladding Applicable to Loss-of-Coolant Accident Conditions in Light-Water Reactors, Zirconium in the Nuclear Industry, ASTM STP681, J. H. Schemel and T. P. Papazoglou, Eds., ASTM International, Philadelphia, PA, 1979, pp. 600-627.

[9] J.C. Brachet, D. Hamon, M. Le Saux, V. Vandenberghe, C. Tofflon-Masclet, E. Rouesne, S. Urvoy, J.L. Béchade, C. Raepsaet, J.L. Lacour, G. Bayon, F. Ott, Study of secondary hydriding at high temperature in zirconium based nuclear fuel cladding tubes by coupling information from neutron radiography/tomography, electron probe micro analysis, micro elastic recoil detection analysis and laser induced breakdown spectroscopy microprobe, Journal of Nuclear Materials 488 (2017) 267-286.

[10] J.C. Brachet, V. Vandenberghe-Maillot, L. Portier, D. Gilbon, A. Lesbros, N. Waeckel, J.P. Mardon, Hydrogen Content, Preoxidation, and Cooling Scenario Effects on Post-Quench Microstructure and Mechanical Properties of Zircaloy-4 and M5™ Alloys in LOCA Conditions, Journal of ASTM International 5 (2008).

[11] O.T. Woo, K. Tangri, Transformation Characteristics of Rapidly Heated and Quenched Zircaloy-4-Oxygen Alloys. Journal of Nuclear Materials 79 (1979) 83-94.

[12] R. Chosson, A.F. Gourgues, V. Vandenberghe, J.C. Brachet, J. Crépin, Creep flow and fracture behavior of the oxygen-enriched alpha phase in zirconium alloys, Scripta Materialia 117 (2016) 20-23.

[13] I. Turque, R. Chosson, M. Le Saux, J.C. Brachet, V. Vandenberghe, J. Crépin, A.F. Gourgues-Lorenzon, Mechanical Behavior at High Temperatures of Highly Oxygen- or Hydrogen-Enriched α and Prior-β Phases of Zirconium Alloys, Zirconium in the Nuclear Industry: 18th International Symposium,

ASTM STP1597, R. J. Comstock and A. T. Motta, Eds., ASTM International, West Conshohocken, PA, 2018, pp. 240-280.

[14] J. Desquines, D. Drouan, S. Guilbert, P. Lacote, Embrittlement of Pre-Hydrided Zircaloy-4 by Steam Oxidation under Simulated LOCA Transients. Journal of Nuclear Materials 469 (2016) 20-31.

[15] S. Guilbert-Banti, P. Lacote, G. Taraud, P. Berger, J. Desquines, C. Duriez, Influence of hydrogen on the oxygen solubility in Zircaloy-4. Journal of Nuclear Materials 469 (2016) 228-236.

[16] A. Pshenichnikov, J. Stuckert, M. Walter, Microstructure and mechanical properties of Zircaloy-4 cladding hydrogenated at temperatures typical for loss-of-coolant accident (LOCA) conditions. Nuclear Engineering and Design 283 (2015) 33-39.

[17] A. Pshenichnikov, J. Stuckert, M. Walter, Hydride precipitation, fracture and plasticity mechanisms in pure zirconium and Zircaloy-4 at temperatures typical for the postulated loss-of-coolant accident. Nuclear Engineering and Design 301 (2016) 366-377.

[18] E. Zuzek, J.P. Abriata, A. San Martin, F.D. Manchester, H-Zr (Hydrogen-Zirconium), Binary Alloy Phase Diagrams 11 (1990) 385-395.

[19] C. Toffolon-Masclet, T. Guilbert, J.C. Brachet, Study of secondary intermetallic phase precipitation/dissolution in Zr alloys by high temperature-high sensitivity calorimetry. Journal of Nuclear Materials 372 (2008) 367-378.

[20] N. Dupin, I. Ansara, C. Servant, C. Toffolon, J.C. Brachet, A Thermo-dynamic Database for Zirconium Alloys. Journal of Nuclear Materials 275 (1999) 287-295.

[21] P. Lafaye, C. Toffolon-Masclet, J.C. Crivello, J.M. Joubert, Experimental investigations and thermodynamic modelling of the Cr-Nb-Sn-Zr system. Calphad 64 (2019) 43-54.

[22] C. Raepsaet, P. Bossis, D. Hamon, J.L. Béchade, J.C. Brachet, Quantification and local distribution of hydrogen within Zircaloy-4 PWR nuclear fuel cladding tubes at the nuclear microprobe of the Pierre Süe Laboratory from μ-ERDA, Nuclear Instruments and Methods in Physics Research B 266 (2008) 2424-2428.

[23] D. Gosset, M. Le Saux, In-situ X-ray diffraction analysis of zirconia layer formed on zirconium alloys oxidized at high temperature, Journal of Nuclear Materials 458 (2015) 245-252.

[24] K. Yan, D.G. Carr, S. Kabra, M. Reid, A. Studer, R.P. Harrison, R. Dippenaar, K.D. Liss, In Situ Characterization of Lattice Structure Evolution during Phase Transformation of Zr- 2.5Nb. Advanced Engineering Materials 13 (2011) 882-886.

[25] R.S. Daum, Y.S. Chu, A.T. Motta, Identification and quantification of hydride phases in Zircaloy-4 cladding using synchrotron X-ray diffraction. Journal of Nuclear Materials 392 (2009) 453-462.

[26] V. Perovic, G.C. Weatherly, C.J. Simpson, Hydride precipitation in α/β zirconium alloys. Acta Metallurgica 31 (1983) 1381-1391.

[27] Z. Zhao, J.P. Morniroli, A. Legris, A. Ambard, Y. Khin, L. Legras, M. Blat-Yrieix, Identification and characterization of a new zirconium hydride. Journal of Microscopy 232 (2008) 410-421.

[28] C. Toffolon, J. Brachet, C. Servant, L. Legras, D. Charquet, P. Barberis, J. Mardon, Experimental Study and Preliminary Thermodynamic Calculations of the Pseudo-Ternary Zr-Nb-Fe-(O,Sn) System. Zirconium in the Nuclear Industry: 13th International Symposium, ASTM STP 1423, American Society for Testing and Materials, West Conshohocken, PA, 2002, pp. 361-383.

[29] H.M. Rietveld, A profile refinement method for nuclear and magnetic structures. Journal of Applied Crystallography 2 (1969) 65-71.

[30] A. Cabrera Salcedo, Modélisation du comportement mécanique "post-trempe", après oxydation à haute température, des gaines de combustible des réacteurs à eau pressurisée. PhD Thesis, MINES ParisTech, France, 2012 (in French).

[31] W.A. Dollase, Correction of intensities for preferred orientation in powder diffractometry: application of the March model. Journal of Applied Crystallography 19 (1986) 267-272.

[32] R.B. Russell, Coefficients of Thermal Expansion for Zirconium. JOM 6 (1954) 1045-1052.

[33] J.G. Couterne, G. Cizeron, Détermination des coefficients principaux d'expansion thermique du Zr α. Journal of Nuclear Materials 20 (1966) 75-82.

[34] J. Goldak, L.T. Lloyd, C.S. Barrett, Lattice Parameters, Thermal Expansions, and Grüneisen Coefficients of Zirconium, 4.2 to 1130°K. Physical Review 144 (1966) 478-484.

[35] S. Yamanaka, K. Yoshioka, M. Uno, M. Katsura, H. Anada, T. Matsuda, S. Kobayashi, Thermal and mechanical properties of zirconium hydride. Journal of Alloys and Compounds, 293-295 (1999) 23-29.

[36] T. Maimaitiyili, A. Steuwer, C. Bjerkén, J. Blomqvist, M. Hoelzel, J.C. Ion, O. Zanellato, The preparation of Zr-deuteride and phase stability studies of the Zr-D system. Journal of Nuclear Materials 485 (2017) 243-252.

[37] G.B. Skinner, H.L. Johnston, Thermal Expansion of Zirconium between 298°K and 1600°K. The Journal of Chemical Physics 21 (1953) 1383-1384.

[38] A. Heiming, W. Petry, J. Trampenau, W. Miekeley, J. Cockcroft, The temperature dependence of the lattice parameters of pure BCC Zr and BCC Zr-2 at.%Co. Journal of Physics: Condensed Matter 4 (1992) 727-733.

[39] G. Aurelio, A. Fernández Guillermet, G. J. Cuello, J. Campo, Structural properties and stability of metastable phases in the Zr-Nb system: Part II. Aging of bcc (β) alloys and assessment of β-Zr. Metallurgical and Materials Transactions A 34 (2003) 2771-2779.

[40] Y. Zhao, J. Zhang, C. Pantea, J. Qian, L.L. Daemen, P.A. Rigg, R.S. Hixson, G.T. Gray, Y. Yang, Y. Wang, Y. Wang, T. Uchida, Thermal equations of state of the α, β, and ω phases of zirconium. Physical Review B 71 (2005) 184119.

[41] K.G. Barraclough, C.J. Beevers, The nature of the γ-phase in zirconium-hydrogen alloys. Journal of the Less Common Metals 35 (1974) 177-179.

[42] S. Mishra, K.S. Sivaramakrihnan, M.K. Asundi, Formation of the gamma phase by a peritectoid reaction in the zirconium-hydrogen system. Journal of Nuclear Materials 45 (1972) 235-244.

[43] B. Nath, G.W. Lorimer, N. Ridley, The relationship between gamma and delta hydrides in zirconium-hydrogen alloys of low hydrogen concentration. Journal of Nuclear Materials 49 (1974) 262-280.

[44] C.D. Cann, E.E. Sexton, An electron optical study of hydride precipitation and growth at crack tips in zirconium. Acta Metallurgica 28 (1980) 1215-1221.

[45] J.H. Root, W.M. Small, D. Khatamian, O.T. Woo, Kinetics of the δ to γ zirconium hydride transformation in Zr-2.5Nb. Acta Materialia 51 (2003) 2041-2053.

[46] W.M. Small, J.H. Root, D. Khatamian, Observation of kinetics of γ zirconium hydride formation in Zr-2.5Nb by neutron diffraction. Journal of Nuclear Materials 256 (1998) 102-107.

[47] Z. Wang, A. Steuwer, N. Liu, T. Maimaitiyili, M. Avdeev, J. Blomqvist, C. Bjerkén, C. Curfs, J.A. Kimpton, J.E. Daniels, Observations of temperature stability of γ-zirconium hydride by high-resolution neutron powder diffraction. Journal of Alloys and Compounds 661 (2016) 55-61.

[48] T. Maimaitiyili, A. Steuwer, C. Bjerkén, J. Blomqvist, M. Hoelzel, J.C. Ion, O. Zanellato, The preparation of Zr-deuteride and phase stability studies of the Zr-D system. Journal of Nuclear Materials 485 (2017) 243-252.

[49] J.E. Bailey, Electron microscope observations on the precipitation of zirconium hydride in zirconium. Acta Metallurgica 11 (1963) 267-280.

[50] J.C. Brachet, C. Toffolon-Masclet, D. Hamon, T. Guilbert, G. Trego, J. Jourdan, A. Stern, C. Raepsaet, Oxygen, Hydrogen and Main Alloying Chemical Elements Partitioning Upon Alpha-Beta Phase Transformation in Zirconium Alloys. Solid State Phenomena 172-174 (2011) 753-759.

[51] P. Boisot, G. Béranger, Variations des paramètres cristallins de la solution solide a zirconium-oxygène en fonction de la teneur en oxygène. Comptes Rendues de l'Académie Des Sciences, Paris - Série C 269 (1969) 587-590.

[52] A. Stern, J.C. Brachet, V. Maillot, D. Hamon, F. Barcelo, S. Poissonnet, A. Pineau, J.P. Mardon, A. Lesbros, Investigations of the Microstructure and Mechanical Properties of Prior-β Structure as a Function of the Oxygen Content in Two Zirconium Alloys. Journal of ASTM International 5 (2008) 1-20.

[53] J.C. Brachet, J.L. Béchade, A. Castaing, L. Le Blanc, T. Jouen, Relationship between crystallographic Texture and Dilatometric Behaviour of a Hexagonal Polycrystalline Material. Materials Science Forum 273-275 (1998) 529-534.

[54] C. Domain, R. Besson, A. Legris, Atomic-scale Ab-initio study of the Zr-H system: I. Bulk properties. Acta Materialia 50 (2002) 3513-3526.

[55] C. Varvenne, O. Mackain, L. Proville, E. Clouet, Hydrogen and vacancy clustering in zirconium. Acta Materialia 102 (2016) 56-69.

[56] A. Hellouin de Menibus, T. Guilbert, Q. Auzoux, C. Toffolon, J.C. Brachet, J.L. Bechade, Hydrogen contribution to the thermal expansion of hydrided Zircaloy-4 cladding tubes. Journal of Nuclear Materials 440 (21013) 169-177.